THE ASTROPHYSICAL JOURNAL, 332:379–399, 1988 September 1

SUBMILLIMETER AND FAR-INFRARED LINE OBSERVATIONS OF M17 SW: A CLUMPY MOLECULAR CLOUD PENETRATED BY ULTRAVIOLET RADIATION

J. STUTZKI,[1,2,3] G. J. STACEY,[4] R. GENZEL,[1,2,3] A. I. HARRIS,[1,2,3] D. T. JAFFE,[2,3,5] AND J. B. LUGTEN[4]

Received 1987 November 13; accepted 1988 February 29

ABSTRACT

We report millimeter, submillimeter, and far-infrared spectroscopic observations of the M17 SW star formation region. Strong [C II] 158 μm and CO $J = 7 \rightarrow 6$ line emission arises in an H II region/molecular cloud interface of several parsecs thickness. Weaker [C II] emission appears to be extended over 15 pc throughout the molecular cloud M17 SW. CO $J = 14 \rightarrow 13$ and [O I] 145 μm spectra indicate high temperatures (200–400 K) and densities (a few 10^4 cm^{-3}) for both molecular and atomic gas in the interface.

The observational results require the molecular cloud near the interface to be clumpy or filamentary. As a consequence, far-ultraviolet radiation from the central OB stellar cluster can penetrate into the dense molecular cloud to a depth of several parsecs, thus creating bright and extended [C II] emission from the photodissociated surfaces of dense atomic and molecular clumps or sheets.

The extended [C II] emission throughout the molecular cloud SW of the M17 complex has a level around 20 times higher than expected from a single molecular cloud interface exposed to an ultraviolet radiation field typical of the solar neighborhood. This suggests that the molecular cloud as a whole is penetrated by ultraviolet radiation and has a clumpy or filamentary structure. The number of B stars expected to be embedded in the M17 molecular cloud probably can provide the UV radiation necessary for the extended [C II] emission. Alternatively, the UV radiation could be external if the interstellar radiation in the vicinity of M17 is higher than in the solar neighborhood.

The high gas temperature of molecular material in the UV-illuminated interface region suggests that CO self-shielding and heating of CO by photoelectrons are important. Comparison of the new submillimeter and far-infrared CO data with emission lines from lower CO levels shows that the molecular cloud structure near the interface is very complex. Temperatures ranging from several ten to several hundred degrees are present. The material has a comparable velocity dispersion throughout this temperature range of 5–10 km s^{-1}.

The picture of a clumpy photodissociation interface implies that emission from neutral atomic carbon should closely follow the distribution of column density of warm CO at the interface. In addition, the UV radiation required to explain the extended [C II] emission is sufficient to sustain a measurable C I abundance throughout the M17 SW molecular cloud.

Subject headings: infrared: spectra — interstellar: molecules — nebulae: individual (M17)

I. INTRODUCTION

Submillimeter and far-infrared spectral line observations during the past few years have revealed a relatively large abundance of warm and dense molecular and atomic material. Strong [C II] 158 μm fine-structure line emission has been found in galactic star formation regions (Russell *et al.* 1980; Russell *et al.* 1981; Kurtz *et al.* 1983; Crawford *et al.* 1985) throughout the inner region of our Galaxy (Stacey *et al.* 1983*b*; Stacey *et al.* 1985), in the Galactic center (Genzel *et al.* 1985; Lugten *et al.* 1986*a*), and toward several external galaxies (Crawford *et al.* 1985; Stacey, Lugten, and Genzel 1987). [O I] 63 μm and 145 μm fine-structure emission from about the same regions indicates that the emitting gas is dense ($n \approx 10^4$–10^5 cm^{-3}) and warm ($T \approx 300$ K; Stacey *et al.* 1983*a*; Crawford *et al.* 1985; Genzel *et al.* 1985; Lugten *et al.* 1986*b*). These observations, together with theoretical models of UV-illuminated clouds (e.g., Langer 1976; Clavel, Viala, and Bel 1978; de Jong, Dalgarno, and Boland 1980; Tielens and Hollenbach 1985), indicate that the fine-structure emission originates predominantly in warm, dense gas at the surfaces of molecular clouds, where an intense flux of far-ultraviolet ($\lambda > 912$ Å) photons from nearby or embedded OB stars, or from the Galactic interstellar radiation field, heats the neutral cloud material via the photoelectric effect.

In the majority of sources observed in the far-infrared to date, large-scale [C II] emission appears to be correlated with CO $J = 1 \rightarrow 0$ emission. This result is somewhat surprising, as the lower rotational transitions of CO presumably trace moderately dense (10^3 cm^{-3}) and cold ($T = 10$–30 K) gas which should be representative of the bulk of the neutral molecular cloud material. Since most centimeter- and millimeter-wave molecular transitions are sensitive only to low temperatures (<100 K), little is known from observations of these transitions about the importance of warm molecular cloud material. Recent CO submillimeter and far-infrared observations now have shown the presence of a significant amount of warm (temperature of a few hundred K), dense ($n_{H_2} \geq$ a few 10^4 cm^{-3}) gas in a variety of sources, ranging from active star formation regions (Jaffe, Harris, and Genzel 1987; Harris *et al.*

[1] Max-Planck-Institut für Physik und Astrophysik, Institut für Extraterrestrische Physik, Garching; and Department of Physics, University of California, Berkeley.

[2] Visiting Observer at the Infrared Telescope Facility, which is operated by the University of Hawaii under contract from the National Aeronautics and Space Administration.

[3] Visiting Observer at the University of Hawaii 88 inch telescope operated by the University of Hawaii.

[4] Department of Physics, University of California, Berkeley.

[5] Department of Astronomy, University of Texas at Austin; and Space Sciences Laboratory, University of California, Berkeley.

1987*b*; Jaffe *et al.* 1987) to the immediate vicinity of the Galactic center (Harris *et al.* 1985; Lugten *et al.* 1986*a*).

In this paper we present a detailed spectroscopic study of several millimeter, submillimeter, and far-infrared lines for an investigation of the physical conditions and excitation requirements of warm, dense material at molecular cloud/H II region interfaces. We selected the M17 SW region for these observations as it is a very well studied complex and is relatively nearby (2.2 kpc; Chini, Elsässer, and Neckel 1980; Crampton, Georgelin, and Georgelin 1978). M17 SW is the most prominent of a series of CO condensations in the M17 molecular cloud complex (Elmegreen and Lada 1976), lying adjacent to a bright H II region. The interface is not resolved with angular resolutions of slightly less than 1′ in either CO $1 \rightarrow 0$ (Thronson and Lada 1983; Martin, Sanders, and Hills 1984) or radio continuum observations (Lada *et al.* 1976; Wilson *et al.* 1979). This indicates that the ionization front is seen almost edge-on. Icke, Gatley, and Israel (1980) estimate from modeling of the far-infrared and radio continuum emission that the ionization front is within 20° of the line of sight.

The M17 H II region is ionized by a highly obscured ($A_v >$ 10 mag) cluster of several OB stars (Beetz *et al.* 1976). The total IR luminosity is (6–7) $\times 10^6\ L_\odot$ (Harper *et al.* 1976; Wilson *et al.* 1979). Far-infrared continuum maps (Gatley *et al.* 1979) show a shift of peak intensity toward the SW with increasing wavelength, indicating a temperature gradient across the interface. Hence, the dust is heated externally by the cluster of young OB stars. The dust temperature is around 50 K in the interface region (Gatley *et al.* 1979). From the measured total flux and distance between the exciting star cluster and the interface ($R = 1.9$ pc) we estimate the flux of far-ultraviolet and visible light at the ionization front to be $2.1 \times 10^2[R(\mathrm{pc})]^{-2}$ ergs s^{-1} cm^{-2} {or $1.3 \times 10^5[R(\mathrm{pc})]^{-2} G_0$ in units of $G_0 = 1.6 \times 10^{-3}$ ergs s^{-1} cm^{-2}; Tielens and Hollenbach 1985}. From the infrared continuum data there is no evidence for other strong internal heating sources in the molecular cloud condensation. Two pointlike, embedded infrared sources, identified by Kleinmann and Wright (1973) and Harper *et al.* (1976), contribute negligibly to the total infrared flux.

Multilevel molecular line observations in CS (Snell *et al.* 1984; Snell *et al.* 1986; Evans *et al.* 1987) and C^{34}S (Mundy *et al.* 1986) suggest that the M17 SW cloud core consists of numerous high-density clumps ($n_{\mathrm{H_2}} > 10^{5.5}$ cm^{-3}). These clumps are embedded in less dense ($\sim 10^{4.5}$ cm^{-3}) material, as derived from H_2CO observations (Mundy 1984; Mundy *et al.* 1987). These densities are derived under the assumption that the molecular material has a temperature of 50 K. That temperature is taken from the almost constant brightness temperature of CO lines up to $J = 4 \rightarrow 3$ in the cloud core, where the emission is optically thick and presumably thermalized (Thronson and Lada 1983; Rainey *et al.* 1987; Schulz and Krügel 1987). Martin, Sanders, and Hills (1984) analyze the $J = 1 \rightarrow 0$ ^{12}CO and ^{13}CO and the $J = 3 \rightarrow 2$ ^{12}CO line profiles in the framework of a clumpy, macroturbulent cloud with an average of ~ 7 fragments along the line of sight.

Recent observations of the [C I] distribution across the M17 SW interface (Keene *et al.* 1985) with 3′ angular resolution find $^3P_1 \rightarrow {}^3P_0$ [C I] emission at 610 μm extended over, and well correlated with, the ^{13}CO $1 \rightarrow 0$ emission region tracing the core of the molecular cloud. Keene *et al.* (1985) conclude from their observations that there is no strong enhancement of [C I] intensity at the H II/molecular interface in contrast to the predictions of photodissociation region models.

II. OBSERVATIONS

The data described in this paper were obtained in a set of seven observing projects: (1) CO $7 \rightarrow 6$ (372 μm) strip maps of about 4′ extent across the molecular cloud/H II region interface, one each in the E-W and NE-SW directions (1′ corresponds to 0.64 pc at the distance of 2.2 kpc); (2) high-resolution, high signal-to-noise ratio CO $7 \rightarrow 6$ spectra at the peak position of these strip maps; (3) a CO $14 \rightarrow 13$ (186 μm) spectrum at the peak position of the FIR continuum emission; (4) a [C II] $^2P_{3/2} \rightarrow {}^2P_{1/2}$ (158 μm) strip map of 60′ extent across the interface in the NE-SW direction; (5) a high spectral resolution [C II] strip map of 4′ extent across the interface in the E-W direction; (6) an [O I] $^3P_0 \rightarrow {}^3P_1$ 145 μm spectrum at the peak position on the E-W strip map; and (7) ^{12}CO and C^{18}O $J = 2 \rightarrow 1$ observations along the CO $7 \rightarrow 6$ strip maps.

The reference position for all our observations is the star SAO 161357 at R.A. (1950) = $18^{\mathrm{h}}17^{\mathrm{m}}34^{\mathrm{s}}.5$, decl. (1950) = −16°13′24″. Offsets are quoted in arcseconds relative to this position. The NE-SW scan direction was defined by stepping 30″ west and 15″ south (and some positions in between) for the high-resolution scans near the interface and by a position angle of 55° east of north for the extended [C II] scan. The E-W direction scan was in 50″ steps for the submillimeter and 30″ steps for the far-infrared data. Figure 1 gives the position and orientation of these scans together with an outline of the radio continuum and the CO $1 \rightarrow 0$ emission.

a) Ground-based Submillimeter Heterodyne Observations

We obtained the submillimeter CO $7 \rightarrow 6$ (806.6517 GHz) data with the UCB/MPE submillimeter heterodyne receiver, consisting of a Schottky diode mixer mounted in a corner cube, a molecular laser local oscillator, and quasi-optical signal coupling. The instrument is described in detail in Harris *et al.* (1987*a*). The CO $7 \rightarrow 6$ strip maps across the interface were obtained on 1985 May 4 with the receiver mounted on the University of Hawaii 88 inch telescope (UH 88) on Mauna Kea, Hawaii. For this observing session the mixer diode was operated at room temperature, and the backend was a filter spectrometer with 64 channels of 200 MHz each, corresponding to 7.4 km s^{-1} velocity resolution at the rest frequency of the CO $7 \rightarrow 6$ line. The beam size at the UH 88 is about 40″ FWHM, derived from the illumination of the telescope. The blockage at the beam center by the large central hole in the primary results in a rather low main-beam efficiency and strong extended sidelobes. The measured beam efficiency was 31% on the (extended) Moon ($T_{\mathrm{Moon}} = 360$ K) and 13% on Jupiter (assuming $T_{\mathrm{Jupiter}} = 130$ K, 39″ diameter uniform disk), the difference being consistent with the calculated beam efficiency for this central blockage (Harris 1987) and the chopper's duty cycle.

The CO $7 \rightarrow 6$ emission extends over $\sim 2'$. Hence, we adopt a main-beam efficiency of 20% to derive Rayleigh-Jeans main-beam brightness temperatures for the strip map data. The resulting main-beam brightness temperatures and integrated intensities are consistent with the more accurately calibrated spectra obtained one year later at the IRTF on the peak position.

The submillimeter data at the IRTF were taken on 1986 May 20 with the same system, except that the mixer diode now was cooled to 77 K, resulting in a 20% better receiver temperature (T_{sys}[DSB] = 4500 K). The backend for these observations was a 1024 channel acousto-optical spectrometer

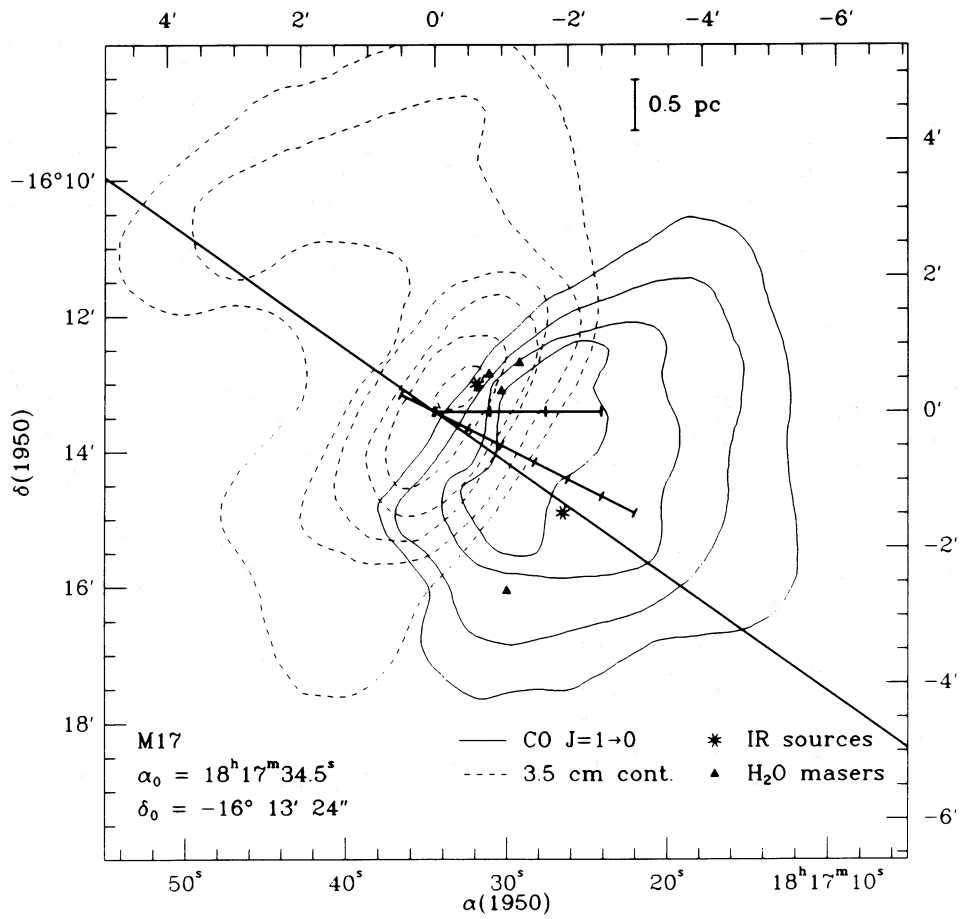

FIG. 1.—Overview of the central area of the M17 SW molecular cloud/H II region complex. The solid straight lines mark the orientation and position of the different strip maps discussed in § II. The two lines with tick marks at position angles 63° and 90° east of north mark the small-scale C^+, ^{12}CO $J = 7 \rightarrow 6$ and ^{12}CO and $C^{18}O$ $J = 2 \rightarrow 1$ scans. The line at position angle 55° marks the large-scale C^+ cut. The H_2O maser source positions (*triangles*) are from Lada *et al.* (1976) and Jaffe, Güsten, and Downes (1981), the IR-source positions (*asterisks*) are from Kleinmann and Wright (1973) and Harper *et al.* (1976).

(AOS) with 600 MHz bandwidth and a velocity resolution of 0.22 km s^{-1} per channel. The beamwidth at the IRTF is 30″ FWHM (measured on scans across the edge of the Moon) and the main-beam efficiency is 55%.

We determined the submillimeter atmospheric transmission approximately hourly by measuring the sky temperature at different zenith angles, assuming a linear sec z dependence of the atmospheric optical depth and a physical sky temperature equal to the ground temperature. Weather conditions were moderate during the observing run at the UH 88 giving a zenith transmission of 15%–20%. Atmospheric transmission along the line of sight toward M17 varied between 8%–15%. We estimate the relative intensity calibration for the CO $7 \rightarrow 6$ strip map to be $\sim 10\%$. During the observations at the IRTF the weather was excellent, giving 30% zenith transmission and accordingly 20%–25% transmission toward the line of sight. The absolute intensity calibration of the CO $7 \rightarrow 6$ data is accurate to within 25%.

The telescope secondary chopped 6′.5 N-S at the UH 88 and 5′ E-W at IRTF. The telescope was nodded after every other scan to cancel beam imbalance. Pointing was checked by a television camera on the boresight. We estimate the overall pointing error to be less than 10″.

b) Airborne Far-Infrared Fabry-Perot Spectroscopy

The far-infrared [C II] (157.7409 μm), [O I] (145.526 μm) and CO $14 \rightarrow 13$ (185.9993 μm) lines were observed with the 91.4 cm telescope on board the NASA Kuiper Airborne Observatory during three flight series in 1985 June, 1986 May, and 1986 July with the University of California at Berkeley Mk II Tandem Fabry-Perot Spectrometer. The instrument is described in detail by Crawford *et al.* (1986) and Lugten (1987). The system noise equivalent power was $(3–5) \times 10^{-15}$ W $Hz^{-1/2}$. For the small-scale strip scan in [C II] the scanning Fabry-Perot was operated in 503d order, giving a velocity resolution of 22 km s^{-1} and for the other observations in 103d order, giving a velocity resolution of 54 km s^{-1}. The instrumental profile is a Lorentzian with an asymmetric shoulder on the long-wavelength side due to the off-axis rays (see Lugten 1987). This shoulder is most prominent in the very high resolution scans. For all far-infrared observations we used a 45″ aperture with an effective FWHM for the beam on the sky of 55″ and a solid angle of 9×10^{-8} sr at 158 μm (10^{-7} sr at 186 μm, 8×10^{-8} sr at 145 μm).

For the extended strip maps across the interface in the NE-SW direction (observed on 1986 July 26 and 28) the tele-

scope secondary was chopped along the scan direction with the offset position toward the SW. The chopper throw was adjusted to the map step size. The final strip map was constructed by adding the incremental changes per step along the scan. The data of five different scans with 5′, 4′, and 2′ step size and different reference points were combined. The different duty cycle for different chopper throws was taken into account by calibrating the individual strip scans versus the 158 μm continuum flux (see below). Checking the data from different step size scans against each other shows that the method gives consistent results. The data from two different observing nights are consistent with each other within the calibration uncertainty of 25%.

The CO 14 → 13 line was observed in 1986 May at 54 km s^{-1} FWHM resolution and 4′ chopper throw (Harris *et al.* 1987*b*). For the 1985 June observations of the [O I] 145.526 μm line (resolution 101 km s^{-1}) and the small-scale [C II] scan, the telescope secondary was chopped 6′ E-W and the telescope was beam switched after every other scan. Pointing was monitored with a television camera along the FIR boresight. We estimate the overall pointing accuracy to be around 10″.

The absolute intensity calibration of the FIR data was derived from the observed continuum level in the spectral line data, extrapolating the 30, 50, and 100 μm continuum data from Gatley *et al.* (1979) to a continuum flux of 7400 Jy in a 50″ beam at 158 μm and 6000 Jy at 186 μm in a 60″ beam. The derived intensity scale was independently checked against planetary observations and was found to be consistent to within 15%.

c) *Ground-based Millimeter Spectroscopy*

The 230.538 GHz $^{12}C^{16}O$ and 219.560 GHz $^{12}C^{18}O$ $J = 2 \rightarrow 1$ transitions were observed in 1987 March with the NRAO 12 m telescope on Kitt Peak.[6] We calibrated the data to the T_R^* scale (Kutner and Ulich 1981) with comparisons of the radiation temperature of the sky to an ambient temperature chopper wheel. On this scale T_R^* at the Orion peak position is 80 K. We checked this scale by making sky temperature measurements at a series of zenith angles. The beam size (FWHM) is 30″. We made a strip map of 2′.5 extent, following the NE-SW CO 7 → 6 scan. The data were taken in position switched scans of 5 minute duration with a reference position carefully selected to be free of CO emission. For these observations, overall pointing uncertainties were about 15″.

III. RESULTS: ATOMIC GAS

a) [C II] *Observations Near the Interface*

The [C II] emission near the H II region/molecular cloud interface originates in a layer of ≥ 1 pc FWHM thickness (Fig. 2). The centroid of the [C II] emission region is located close to, but somewhat outside of, the region of most intense radio continuum emission. The [C II] emission drops off rather smoothly toward the molecular cloud. The average [C II] intensity level within the region of strong CO 7 → 6 emission (see below) is still half the peak value.

[6] The National Radio Astronomy Observatory is operated by Associated Universities, Inc., under contract with the National Science Foundation.

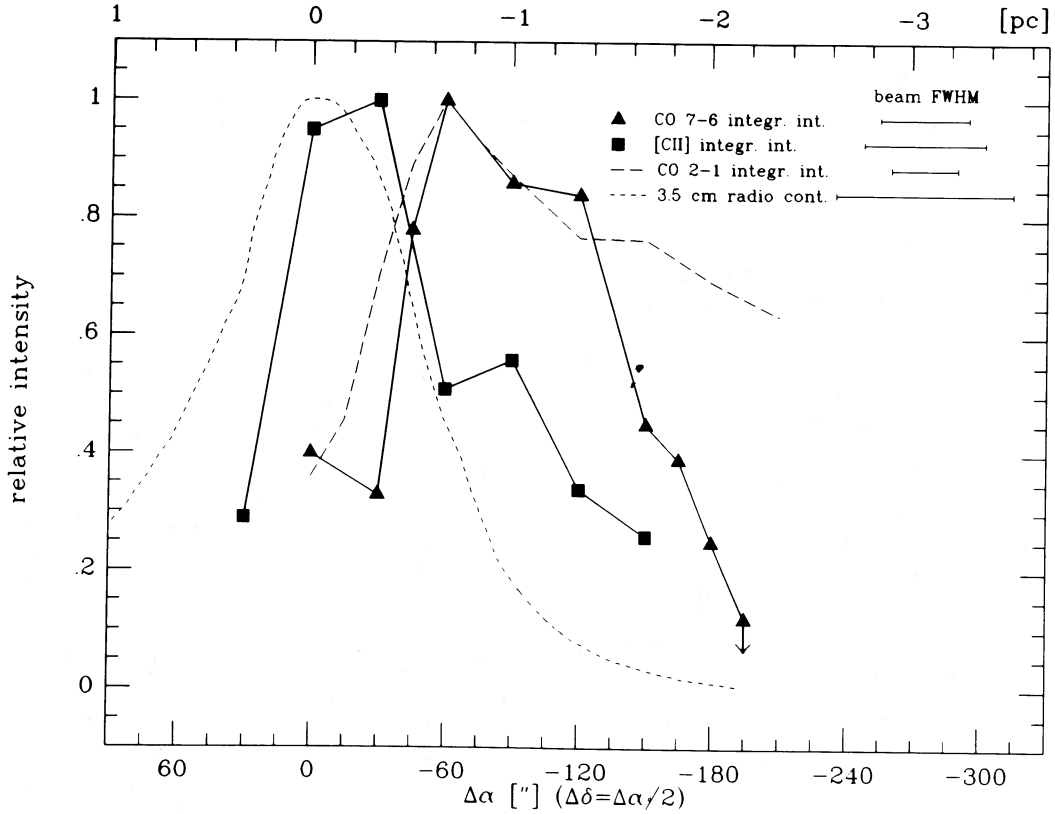

FIG. 2.—Integrated [C II] (158 μm), CO $J = 7 \rightarrow 6$ (372 μm, 806.652 GHz), and CO $J = 2 \rightarrow 1$ (230.538 GHz) intensity distribution along the short NE-SW strip scan (see Fig. 1). The radio continuum intensity distribution at 3.5 cm (Wilson *et al.* 1979) is shown for comparison.

The [C II] emission from the H II region molecular cloud interface is, like the molecular lines, centered near 20 km s^{-1}, the velocity of the molecular cloud complex. The line is, however, wider than the molecular lines observed at the interface. The average profile of four [C II] spectra near the [C II] peak (shown in Fig. 3) has an observed full width at half-maximum of ~ 40 km s^{-1}. The instrumental profile, a modified Lorentzian as discussed above, has a FWHM of slightly less than 25 km s^{-1}. An estimate of the intrinsic [C II] line profile is given in Figure 3, after deconvolution of the data in Figure 3 with the maximum entropy method (Gull and Daniell 1978; Crawford *et al.* 1986). The profile is dominated by intense emission centered near $v_{LSR} \approx 15$ km s^{-1} (FWHM ≤ 25 km s^{-1}) with an asymmetric shoulder of emission extending to $v_{LSR} \approx 40$ km s^{-1}. No systematic variations of the line center or width are detectable in our data. There are several possible explanations why the [C II] line width is larger than the width of the molecular emission lines and why it is centered at a smaller velocity.

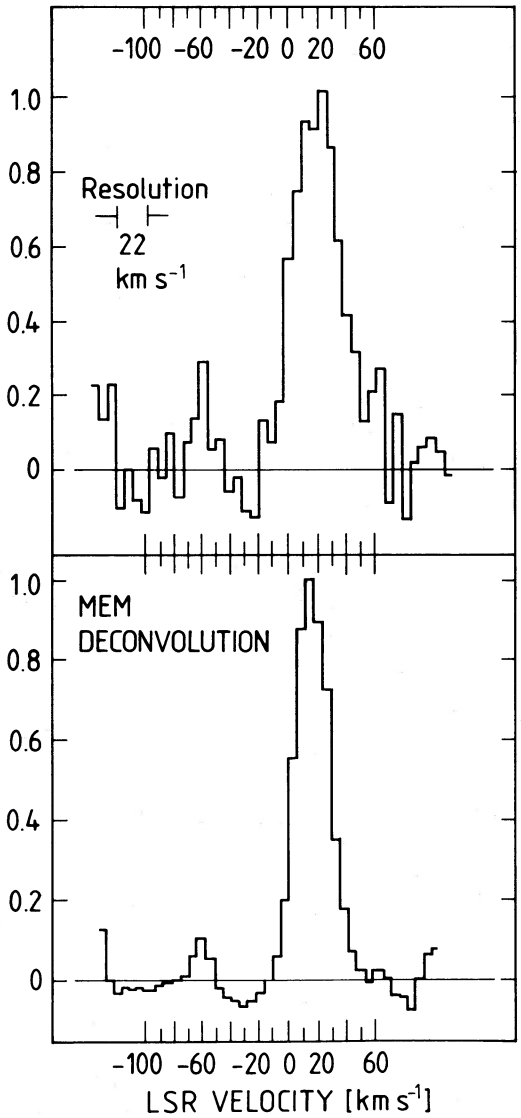

FIG. 3.—[C II] 158 μm profile. *Top*: Observed [C II] 158 μm spectrum averaged over four position in M17 close to the emission peak. The instrumental profile is a modified Lorentzian with asymmetric long wavelength (FWHM $\approx$ 22–25 km s^{-1}). *Bottom*: The MEM deconvolved spectrum.

First, the observed line profile could be affected by self-chopping onto the source. There are some variations between the [C II] intensities from the two chop sides, but probably not large enough to explain the [C II] line profile as a result of self-chopping. Furthermore, the integrated intensities of the [C II] emission at the peak taken with different chop amplitudes do not differ by more than about 30%. Second, the line profile could result from self-absorption of the [C II] emission near the interface by cooler, line-of-sight ionized carbon further away from the interface. The optical depth of the weaker, large-scale (15 pc) [C II] emission in M17 discussed below, for example, could be significant. The effects of lower gas temperature and smaller velocity spread in that extended component may balance or outweigh the lower intensity relative to the bright interface emission, thus resulting in about the same or larger optical depth than in the bright [C II] emission component ($\tau \approx 0.2$–1; see Crawford *et al.* 1985 for relevant formulae). Radiative transport of the [C II] emission through such an extended, cooler C^+ region could thus affect the line profile of the bright [C II] line from the interface.

Third, much of the [C II] intensity at the interface may come from dense, mostly atomic clumps at the edge of the H II region, as is suggested by the proximity of [C II] and radio continuum peaks. The small-scale scans (Fig. 2) show that the peak of the [C II] emission is closely associated with ionized gas, while there appears to be little molecular column density as inferred from the $C^{18}O$ intensity (see Fig. 9 below). Felli, Churchwell, and Massi (1984) have shown that the radio emission from the H II region has a very clumpy structure on the arcsecond scale. The dense atomic clumps near the interface with ionized surfaces of high emission measure may be the remains of originally molecular material which has been dissociated and partly ionized by the expanding H II region. The large line width of the [C II] emission could then indicate that part of the [C II] emission originates in material which has acquired the much higher turbulent velocities inside the H II region and which may be evaporating off the dense molecular cloud interface. The [C II] line width falls in between the line width of the molecular cloud material (≤ 10 km s^{-1}) and that of the ionized gas (40–50 km s^{-1}) traced in optical forbidden lines (Elliot and Meaburn 1975).

The [C II] emission cannot come from the ionized gas of the M17 H II region, as has been demonstrated previously for other H II regions (Russell *et al.* 1981; Stacey 1985). The H II region has an electron density of around 700 cm^{-3} (Schraml and Mezger 1969; Watson *et al.* 1981), and the ratio of He II to H II column densities of 0.09 implies a high enough temperature of the radiation field for carbon to be almost completely doubly ionized. We estimate that the [C II] intensity from the ionized gas within the H II region is less than 2×10^{-4} ergs s^{-1} cm^{-2} sr^{-1}, more than an order of magnitude less than the observed intensity.

b) [C II] *Emission at Larger Scales*

The large-scale [C II] distribution (Fig. 4) measured along a strip scan of $\sim 60'$ (40 pc) extent in the NE-SW direction shows a quasi-exponential tail of [C II] emission reaching into the molecular cloud. The data imply that the neutral gas in M17 SW must be clumped or filamentary. A detailed model of the [C II] distribution will be discussed below.

Considering that the penetration depth of UV radiation is

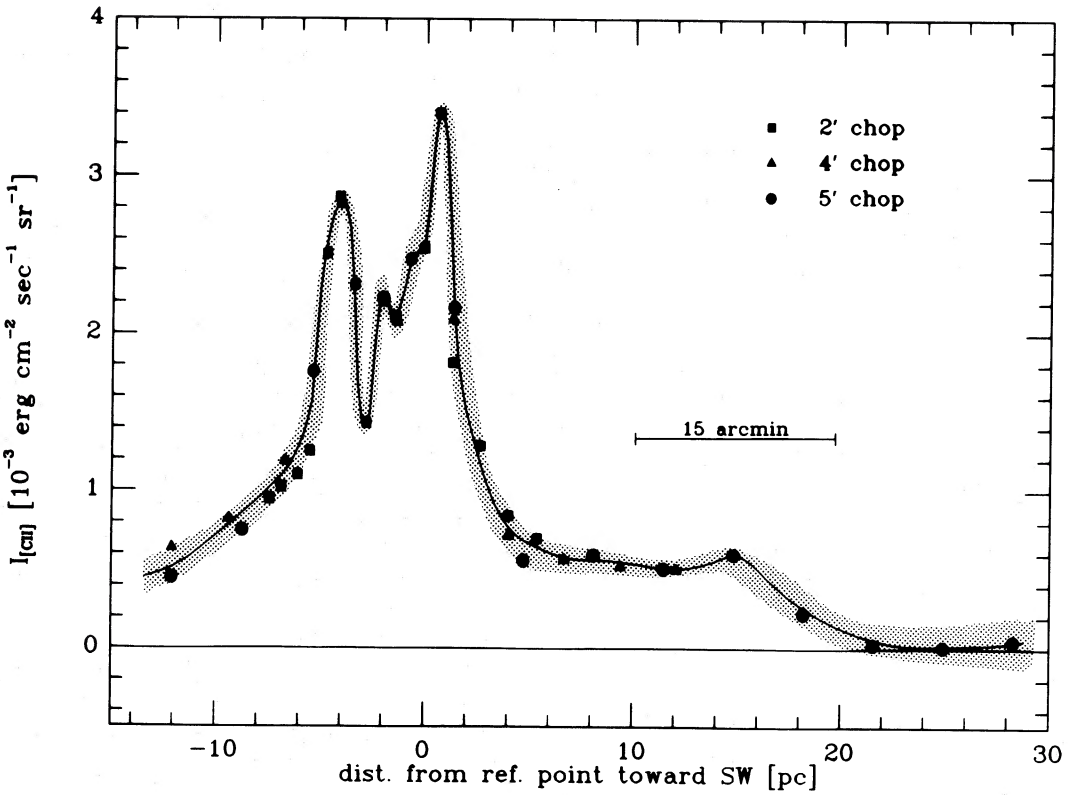

FIG. 4.—The large-scale NE-SW [C II] 158 μm strip map along position angle 55° (see Fig. 1) with almost 1° angular extent on the sky. The data are reconstructed from integration of individual, spatially chopped scans with chopper throws of 2', 4', and 5', respectively, and with the reference beam position on the next position along the scan.

$A_v \leq 3$ (in between the 912–1101 Å hydrogen and carbon ionization edges), corresponding to an H_2 column density of $\leq 6 \times 10^{21}$ cm^{-2}, the observed attenuation length of around 3' or 2 pc is equivalent to an average hydrogen density of slightly less than 10^3 cm^{-3}. Volume densities of molecular hydrogen estimated from excitation of molecular lines are $\geq 4 \times 10^4$ cm^{-3}. however, and the mean volume density estimated from $C^{18}O$ column density and cloud size is $\sim 2 \times 10^4$ cm^{-3}. Furthermore, the extinction through the interface in the visible, as estimated from the dust optical depth at 50 μm (Gatley *et al.* 1979), is 100 mag ($N_{H_2} \approx 2 \times 10^{23}$ cm^{-2}). Hence, the spatial distribution of the [C II] 158 μm radiation can only be explained if the molecular gas is clumped with a surface-to-volume ratio which is more than an order of magnitude larger than in a homogeneous cloud.

Inclination against the line of sight or a curved geometry can only contribute a minor part of the 3 pc extent of the region of peak [C II] emission. The line-of-sight extent of the M17 SW core is about 2 pc, either estimated from the column density of a few times 10^{23} cm^{-2} and the average density of a few times 10^4 cm^{-3}, or by extrapolating from the lateral extent NW-SE. Thus, in order to bring the line-of-sight and NW-SE extent of the cloud core into agreement with the observed size across the interface, an inclination angle on the order of 45° would be required. Such a large inclination angle, however, seems to be very unlikely considering the very sharp boundary between radio continuum and molecular emission or the very sharp increase in intensity for the [C II] and warm molecular emission (see below) at the interface.

Another [C II] interface is located northeast of the H II region. The second interface shows [C II] emission of overall extent 5'–10', which is in good agreement with the size of the [C II] "halo" originally discovered by Russell *et al.* (1981) at 6' resolution. Convolution of our data with their 4' × 7' beam gives a flux of 4.3×10^{-2} W m^{-2}, which is within 30% of the value measured by Russell *et al.* (1981). Molecular material is present in the northeast as well and is traced by continuum maps of far-infrared dust emission (Gatley *et al.* 1979; Wilson *et al.* 1979) and ^{12}CO maps in $J = 1 \rightarrow 0$ (Sanders *et al.* 1985; Gatley and Kaifu 1987) and $3 \rightarrow 2$ (Rainey *et al.* 1987). The H_2 column density in this region, estimated from the dust optical depth at 50 μm, is ~ 20 times lower than in the SW cloud, i.e., $\sim 10^{22}$ cm^{-2}. Again, the UV radiation penetrates the cloud to a greater depth than would be consistent with a homogeneous cloud of neutral material with this average column density. As on the southwestern side, the neutral material must be clumpy or filamentary.

In addition to [C II] emission from either side of the H II region, the extended [C II] scan gives strong evidence for [C II] emission from throughout the molecular cloud (scale size is ~ 15 pc; Fig. 4). The reconstruction of the [C II] large-scale intensity distribution comes from integration of chopped (difference) data as displayed in Figure 5 for two of the five scans. The detection of the extended [C II] emission in our data relies mainly on the spectrum at position offset +27' southwest on the extended scan, where the [C II] emission changes significantly. There is also a weaker positive signal at position offset +32'. The positive signal at +27' is significant at more than the 5 σ level as estimated from the noise in the baselines. Since there is no indication for a negative signal in the vicinity of that position, we interpret the positive emission at +27' as a change in base level between the emission at offsets +7' to +22' and

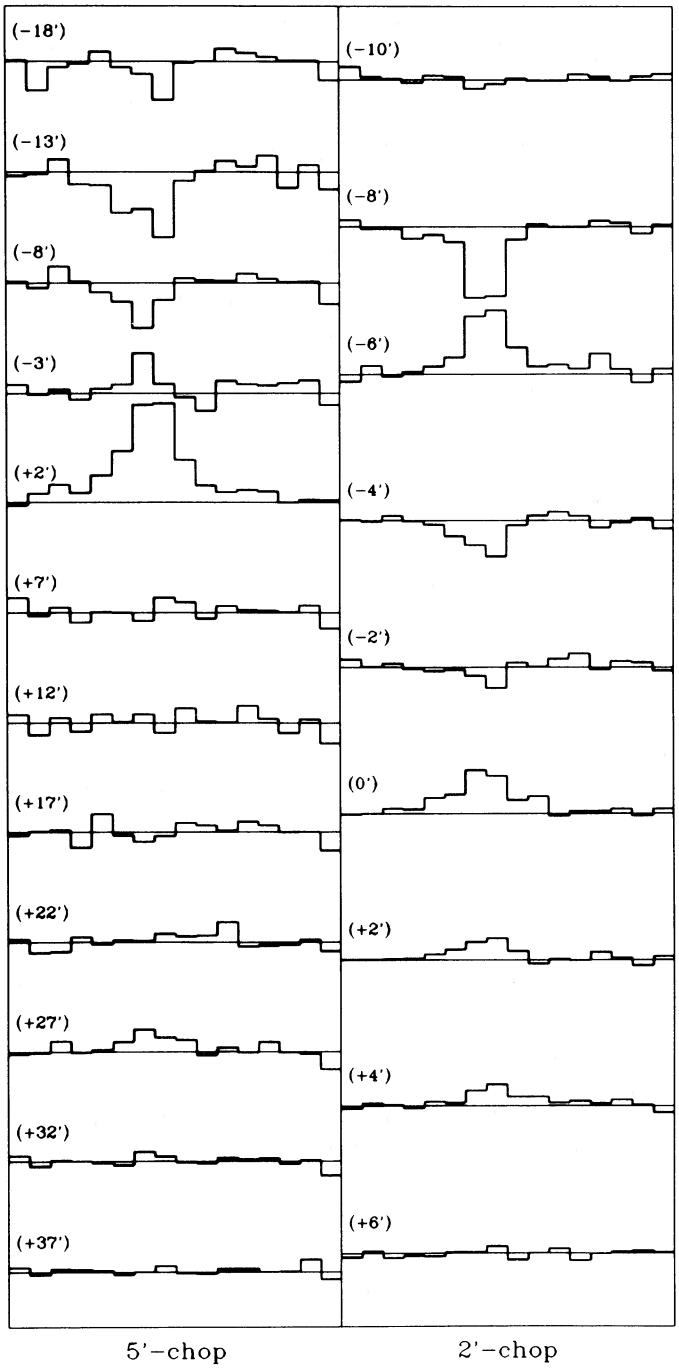

FIG. 5.—Individual "raw" [C II] 158 μm spectra for two of the five extended cuts leading to the reconstructed distribution in Fig. 4. The positions are given as offsets in arcminutes toward the SW from the (0,0) position. Typical integration time is 2 minutes per position. The velocity resolution chosen was ~ 60 km s^{-1} so that the profiles shown are unresolved.

the emission at +32′ and +37′ and hence as strong evidence for very extended [C II] emission. The extended [C II] emission is similarly distributed as the CO 1 → 0 intensity distribution near $v_{LSR} \approx 20$ km s^{-1} (Fig. 6; Elmegreen and Lada 1976; Sanders *et al.* 1985). Its intensity (5×10^{-4} ergs cm^{-2} s^{-1}) is around 20 times higher than the intensity predicted for the surface of a typical giant molecular cloud complex exposed to the averaged interstellar UV field in the solar neighborhood (Takahashi, Tielens, and Hollenbach 1987; de Jong, Dalgarno, and Boland 1980).

c) [O I] *Observations*

Comparison of different atomic fine-structure lines allows an estimate of temperature and density of the emitting gas. We measured an [O I] 145 μm intensity of 5.5×10^{-11} ergs s^{-1} cm^{-2} at the peak position (100W, 0S) of the [C II] emission. This intensity, when compared to the [O I] 63 μm intensity of 2×10^{-10} ergs s^{-1} cm^{-2} (Tielens, private communication; scaled for the different beam sizes) gives an $[\mathrm{O\ I}]_{63\ \mu m}/[\mathrm{O\ I}]_{145\ \mu m}$ intensity ratio of ~ 3.5. Such a low ratio indicates that the [O I] 63 μm line is optically thick. The $[\mathrm{O\ I}]_{145\ \mu m}/[\mathrm{C\ II}]_{158\ \mu m}$ intensity ratio is 0.17. If additionally constrained by the assumption that the interface region has a pressure comparable to that of the H II region of $n_{\mathrm{H\ I}}\ T \approx 10^7$ cm^{-3} K, this ratio gives a temperature ~ 250 K and a density $\sim 10^{4.5}$ cm^{-3} (Watson 1984). Though this is a rough estimate, these values are very close to the temperature and density estimated for the warm molecular material on the molecular side of the interface derived by comparing different CO transitions.

IV. RESULTS: MOLECULAR GAS

a) *Submillimeter and Far-Infrared* CO *Observations*

The CO 7 → 6 emission is centered near 20 km s^{-1} with a line width of ~ 5 km s^{-1} at the peak of the NE-SW scan at (60W, 30S) and ~ 8.5 km s^{-1} at the peak on the E-W scan at (100W, 0S), close to the far-infrared continuum peak (see Fig. 7 here and Fig. 1 in Harris *et al.* 1987*b*). The center velocity thus agrees well with the velocity of the molecular cloud observed in CO 1 → 0 and other millimeter- and centimeter-wave lines. The line width of the CO 7 → 6 emission, however, is narrower than the width of lower J CO lines. There is no indication for the existence of additional discrete velocity components comparable to those found in CO 2 → 1 and 3 → 2 at v_{LSR} around 12 and 30 km s^{-1} (Fig. 8 and Rainey *et al.* 1987). NH_3 inversion transitions at 1.3 cm show emission in two velocity features at 19.5 and 21 km s^{-1} near the interface (Güsten, private communication). Those components, however, are separated by only 2 km s^{-1} with line widths of ~ 1.5 km s^{-1} and therefore would not be resolvable as separate components in the CO 7 → 6 emission with a total line width of 5–10 km s^{-1}. The CO 14 → 13 line is unresolved at the instrumental resolution of 54 km s^{-1}, implying that the line itself is not wider than about 25 km s^{-1}. The CO 14 → 13 line centroid is also at 20 km s^{-1}.

Harris *et al.* (1987*b*) have discussed the implications of the absolute and relative intensities of the submillimeter and far-infrared CO emission for the physical conditions of the molecular gas in the M17 interface. For completeness, we briefly summarize their results here again: (1) the 7 → 6 Rayleigh-Jeans line brightness temperature (85 K) at the peak position (60W, 30S) shows that the kinetic temperature of the emitting gas is greater than 100 K; (2) in a single-temperature cloud model the ratio of $J = 14 \rightarrow 13$ to $7 \rightarrow 6$ intensities at the far-infrared continuum peak position (100W, 0S) implies a gas pressure $n_{H_2} T$ around 10^7 cm^{-3} K at a minimum beam-averaged CO column density of 6×10^{17} cm^{-2}; (3) lower column densities are not sufficient to produce the observed brightness of the CO 7 → 6 line. Higher column densities require somewhat less pressure due to line trapping (4×10^6 cm^{-3} K at 6×10^{18} cm^{-2} column density; (4) the most likely values for temperature and density are around 250 K and 4×10^4 cm^{-3} at a beam-averaged column density of 2×10^{18} cm^{-2}.

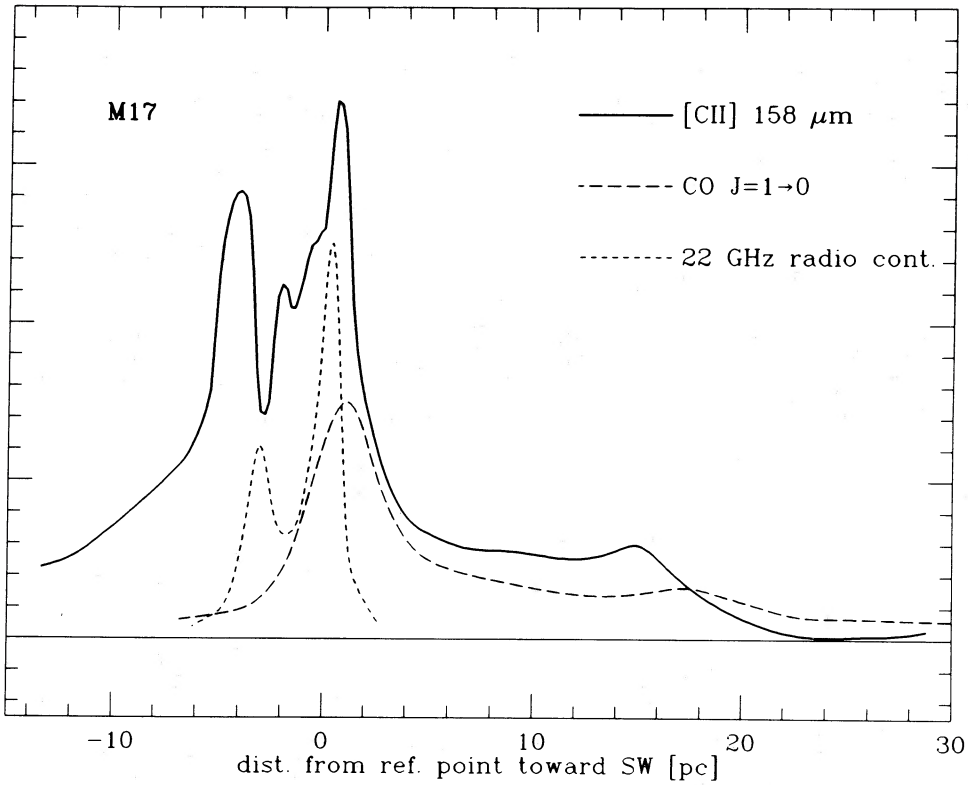

FIG. 6.—Comparison of the large-scale [C II] 158 μm emission with the radio continuum 22 GHz distribution (Lada *et al.* 1976) and integrated CO $J = 1 \rightarrow 0$ intensity between LSR velocities of 15–25 km s^{-1} (Sanders *et al.* 1985).

At the lowest possible column density, the $7 \rightarrow 6$ line has an optical depth slightly less than 1 and is still somewhat subthermally excited. The intrinsic brightness temperature of this gas is only slightly higher than the observed one. A beam filling factor near unity is required to explain the observed brightness. At higher column densities, the $7 \rightarrow 6$ line is optically thick and thermalized, and a beam filling factor of 30% to 60% can explain the observed brightness temperature.

As seen from the CO $7 \rightarrow 6$ strip map (Fig. 2), the warm, dense molecular component, like the [C II] emission, comes from a layer about 100″ (1.1 pc) thick between the H II region and M7 SW molecular cloud. The CO $J = 7 \rightarrow 6$ emission peak is located ~30″ behind the centroid of the [C II] emission region. Just beyond the ionization front, the submillimeter CO emission increases by a factor of 4 to peak intensity within 1 beamwidth: the interface to the H II region is very sharp, confirming that the interface is seen almost edge-on. Toward the core of the molecular cloud the $J = 7 \rightarrow 6$ emission drops off only somewhat more slowly (Fig. 2). The distribution along the E-W scan looks very similar. The region of peak intensity lies directly outside the H II region, as traced by its radio continuum emission. The CO $7 \rightarrow 6$ emission region represents the edge of the molecular cloud as traced by the CO $J = 2 \rightarrow 1$ emission (with comparable angular resolution). The data do not show any significant positional shift between the CO $7 \rightarrow 6$ distribution and the enhanced $J = 2 \rightarrow 1$ emission at the cloud edge (see below).

b) *Millimeter-Wave* CO *Observations*

The ^{12}CO $J = 2 \rightarrow 1$ spectra along the NE-SW cut (30″ resolution, Fig. 8) show a very complex velocity structure: in addition to a feature of width 10 km s^{-1} centered near 20 km s^{-1} v_{LSR} where is a feature at $v_{LSR} \approx 11$ km s^{-1} peaking near the maximum of the radio continuum emission in front of the 20 km s^{-1} molecular cloud. This feature has also been seen by Rainey *et al.* (1987) in ^{12}CO $J = 3 \rightarrow 2$. It is not visible, however, in the $C^{18}O$ $J = 2 \rightarrow 1$ line, implying a lower column density than the 20 km s^{-1} feature.

The $C^{18}O$ $J = 2 \rightarrow 1$ emission, on the other hand, has very simple profiles with the line center near $v_{LSR} = 20$ km s^{-1}, Δv(FWHM) = 5 km s^{-1} (Fig. 8). The distribution of integrated $C^{18}O$ $J = 2 \rightarrow 1$ emission (Fig. 9) is very similar to the ^{12}CO $J = 7 \rightarrow 6$ submillimeter emission distribution, implying that the interface region is also a very sharp CO column density peak.

The peak $C^{18}O$ $2 \rightarrow 1$ main-beam brightness temperature of 8 K at position (60W, 30S) and line width of 4.8 km s^{-1} (FWHM) imply a beam-averaged column density in the $J = 2$ state of $C^{18}O$ equal to

$$\eta_f N_{J=2}(C^{18}O) = 1.5 \times 10^{14}\ \mathrm{cm}^{-2} T_B(\mathrm{K})\ \Delta v\ (\mathrm{km\ s}^{-1}) = 5.8 \times 10^{15}\ \mathrm{cm}^{-2}, \quad (1)$$

where η_f is the beam filling factor, N_J is the column density in level J, T_B is the Planck-corrected main-beam brightness temperature, and Δv is the line width (FWHM).

With a partition function $Q(T) \leq kT/hB$ (B is the molecular rotational constant), this corresponds to a beam-averaged total $C^{18}O$ column density of

$$\eta_f N(C^{18}O) = Q(T)\eta_f N_{J=2} \exp(E_{J=2}/kT)/g_{J=2} \leq 4.4 \times 10^{14}\ \mathrm{cm}^{-2} \exp[15.8/T(\mathrm{K})] \times T(\mathrm{K}). \quad (2)$$

E_J is the energy above ground state of level J, g_J is the sta-

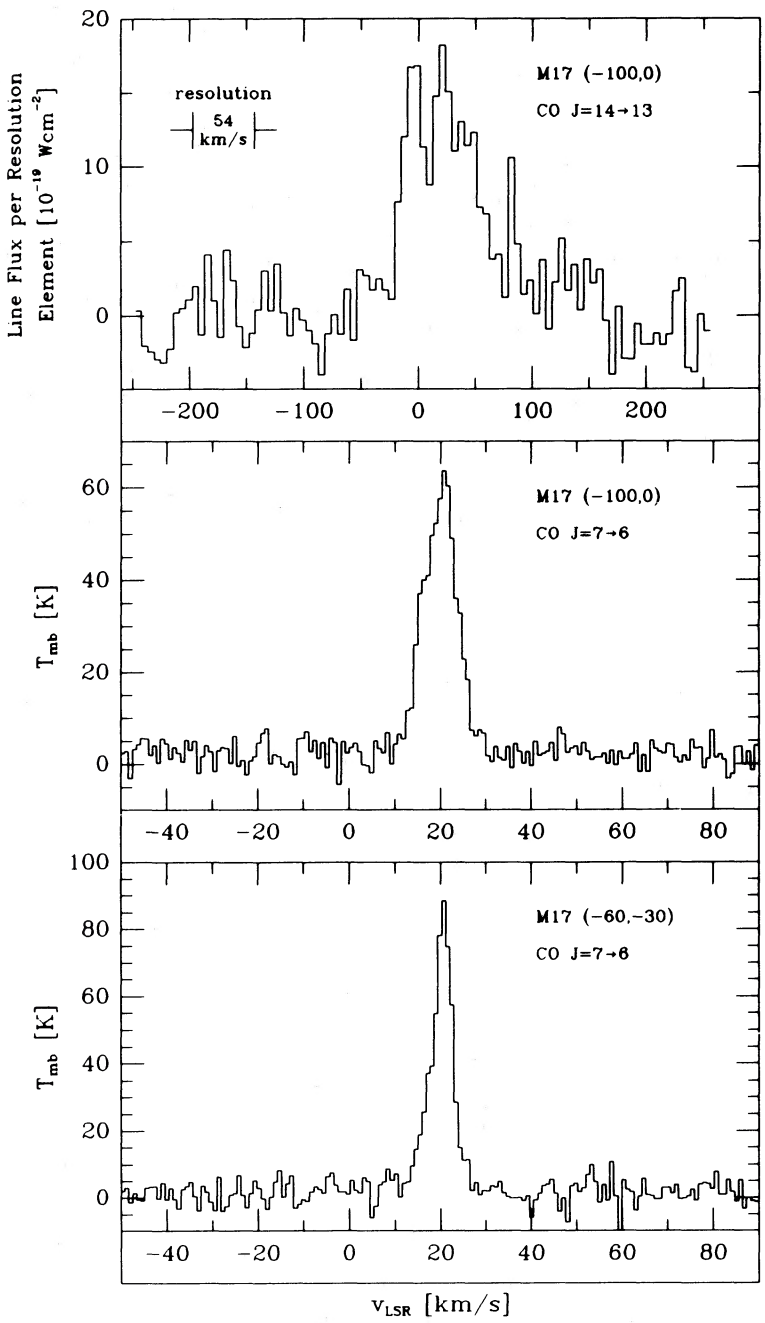

FIG. 7.—$J = 7 \rightarrow 6$ (372 μm) and $14 \rightarrow 13$ (186 μm) CO spectra toward the positions of peak $7 \rightarrow 6$ intensity in M17 (from Harris *et al.* 1987*b*). Spectra at position (100W, 0S) are at top and middle, and the spectrum at position (60W, 30S) is at bottom. Position offsets are in arcseconds relative to the base position at R.A. = $18^h17^m34^s.5$, Decl. = $-16°13'24''$ (1950).

tistical weight, and T is the kinetic temperature. The resulting $C^{18}O$ column density is 3.0×10^{16} cm^{-2} for 50 K, or 5.2×10^{16} cm^{-2} for 100 K temperature. The 30″ beam-averaged $C^{18}O$ $J = 2 \rightarrow 1$ optical depth is $0.16/\eta_f$ to $0.08/\eta_f$. With a $[^{12}CO]/[C^{18}O]$ abundance ratio of 500, the material visible in the $C^{18}O$ line therefore corresponds to a ^{12}CO beam-averaged column density of (1.5–2.6) $\times 10^{19}$ cm^{-2}. This is consistent with column densities estimated from ^{13}CO observations by Thronson and Lada (1983) and from the far-infrared dust optical depth (Gatley *et al.* 1979).

The values for CO column density derived at position (100W, 0S), the CO $7 \rightarrow 6$ peak position on the E-W scan, are the same as those at (60W, 30S) within 15%. At the derived beam-averaged column density the ^{13}CO $J = 2 \rightarrow 1$ line (Plambeck, private communication) has an optical depth of 0.8 (at 50 K) and the observed $C^{18}O$-to-^{13}CO intensity ratio of 0.3, as well as the ^{12}CO-to-^{13}CO intensity ratio of 2.0, is in reasonable agreement with the assumed abundance ratios $[^{13}CO]/[C^{18}O] = 7$ and $[^{12}CO]/[^{13}CO] = 70$. The predicted ^{13}CO $J = 2 \rightarrow 1$ to $1 \rightarrow 0$ intensity ratio is 25% higher than the observed ratio of 1.3.

Given the large column densities implied by the ^{13}CO and

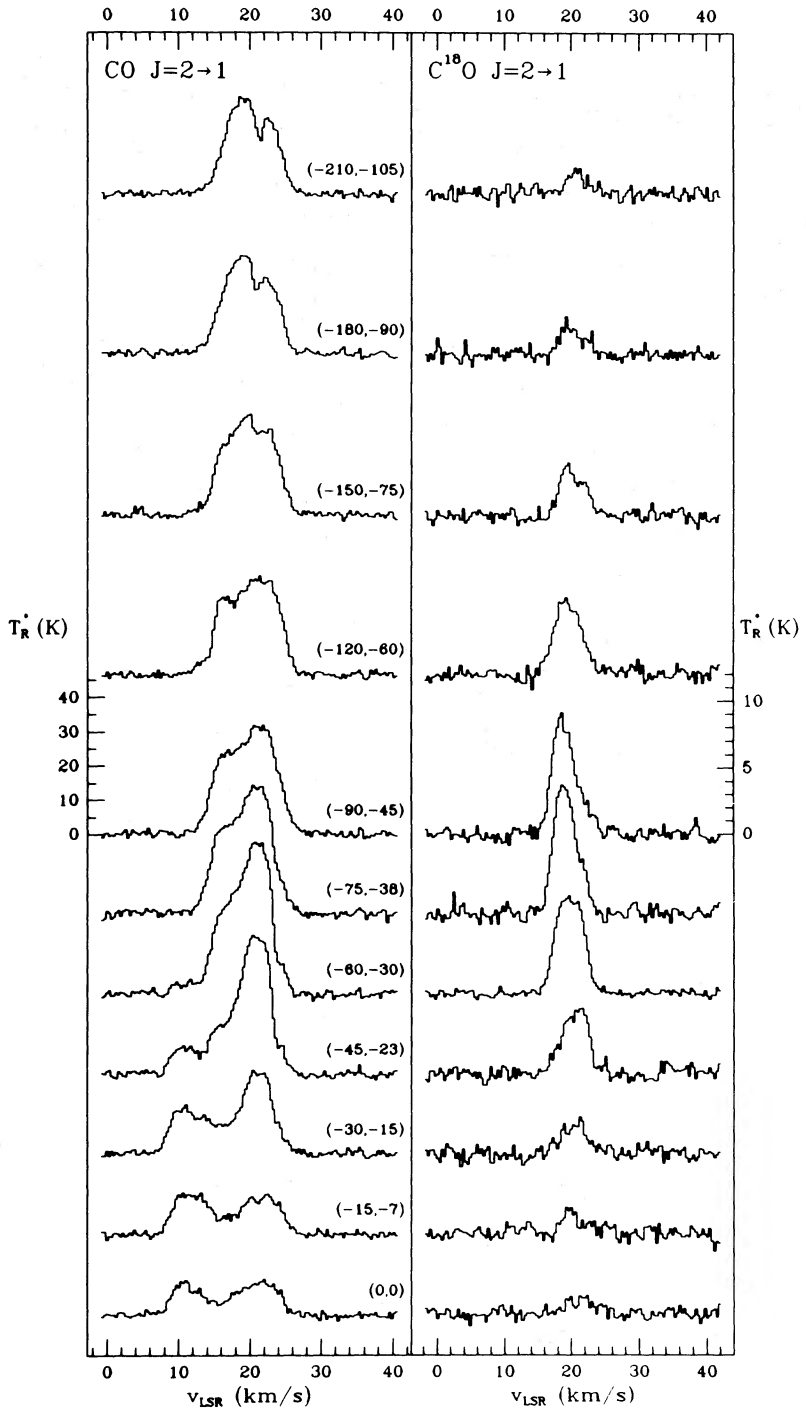

FIG. 8.—^{12}CO and C^{18}O $J = 2 \rightarrow 1$ spectra along the short NE-SW strip scan (see Fig. 1) taken with a 30″ (FWHM) beam. Position offsets are in arcseconds from the base position.

C^{18}O lines, the lower J ^{12}CO lines have very high optical depth ($\tau[^{12}\text{CO } 1 \rightarrow 0] = 20$–$50$). The ^{12}CO line profiles are thus very sensitive to small amounts of gas along the line of sight and probably do not trace the bulk of the molecular cloud material. This conclusion is supported by the comparison of ^{12}CO to C^{18}O $J = 2 \rightarrow 1$ line profiles (Fig. 10) and the evidence for self-absorption in the ^{12}CO $2 \rightarrow 1$ and $3 \rightarrow 2$ lines (Fig. 8 and Rainey *et al.* 1987).

V. THE STRUCTURE OF THE INTERFACE: A CLUMPY OR FILAMENTARY PHOTODISSOCIATION REGION

The high angular resolution scans in the [C II] 158 μm and CO $7 \rightarrow 6$ transition (Fig. 2) qualitatively show a distribution expected for a photodissociation region seen almost edge-on. The ionized carbon layer lies next to the H II region (Figs. 2 and 6). Further into the molecular cloud is a warm molecular layer, followed by cool molecular material. The observed

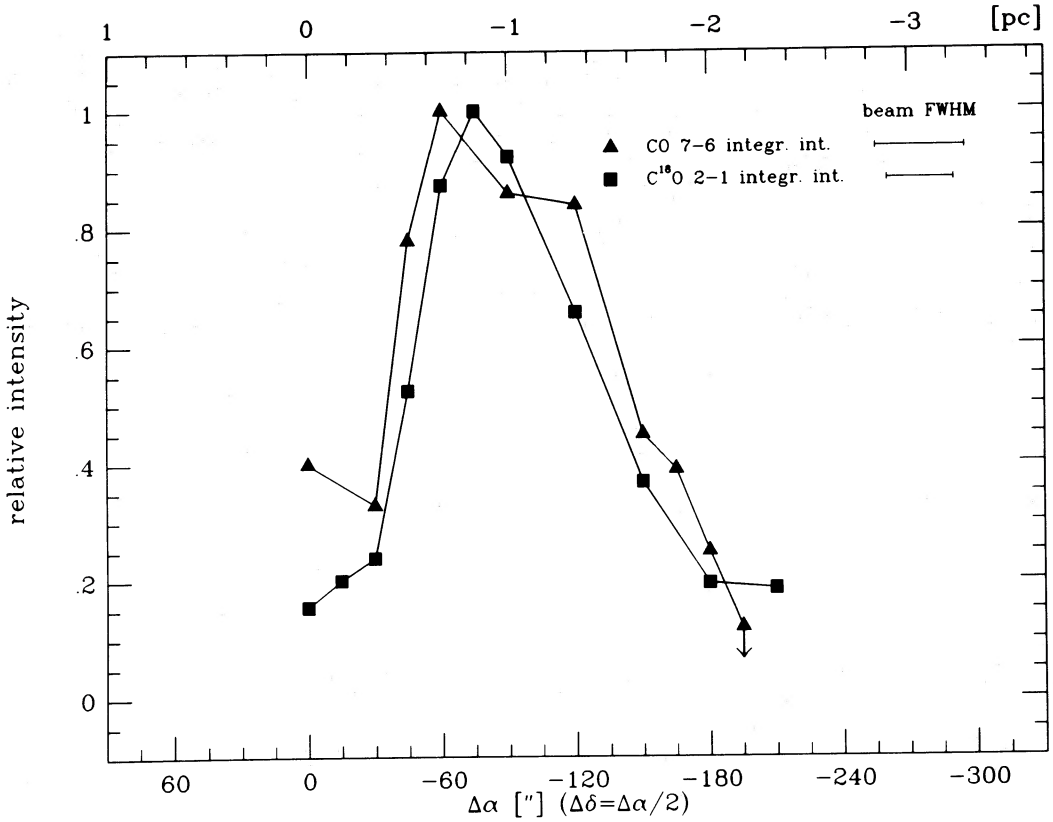

FIG. 9.—Comparison of velocity-integrated CO $J = 7 \rightarrow 6$ and $C^{18}O$ $J = 2 \rightarrow 1$ intensity along the short NE-SW strip map (position angle 63°)

beam-averaged column density of carbon is constant to within a factor of 3 throughout the interface region. With the temperature and density derived above from the [O I]/[C II] intensity ratio, the observed [C II] intensity requires a [C II] beam-averaged column density of at least $\sim 4 \times 10^{18}$ cm^{-2} in the optically thin limit. With the derived excitation conditions the [C II] line is close to optically thick ($\tau \leq 1$) at this column desnsity (see eq. [A5] in Crawford *et al.* 1985). This column density is comparable to the sum of the warm and cool CO column densities at the peak of the CO $7 \rightarrow 6$ emission: the warm CO beam-averaged column density is around 10^{18} cm^{-2} as derived above from the excitation requirements; the cooler molecular material at this position has a beam-averaged column density around 10^{19} cm^{-2} as derived from the optically thin $C^{18}O$ $J = 2 \rightarrow 1$ line.

Line intensities of [C II] and [O I] fine-structure lines are also in good agreement with photodissociation models for high-UV energy densities (Tielens and Hollenbach 1985). Mechanisms creating C^+ ions without ultraviolet radiation such as shocks (Hill and Hollenbach 1978; Hollenbach and McKee 1979) or cosmic rays (Prasad and Tarafdar 1983) fail by several orders of magnitude in explaining both small- and large-scale [C II] emission. There are, however, several important differences between the observational results and, for example, the Tielens and Hollenbach (1985) models. First, the [C II] and warm CO emission regions have a transverse diameter at least 10 times larger than predicted in the theoretical models of one-dimensional, homogeneous interfaces. Second, the peak position of [C II] emission in front of the warm CO emission region is almost coincident with the radio continuum emission region. Third, the warm CO emission region (projected on the sky) is coexistent with the region of maximum CO column density (traced by the $C^{18}O$ $J = 2 \rightarrow 1$ line) which mostly contains gas of lower temperatures. Finally, the warm CO gas has a much higher temperature than predicted in the theoretical models.

The spatial extent of the photodissociation region (2–3 pc), the overlap of [C II] emission with the H II region, and the similar angular distribution of CO $J = 7 \rightarrow 6$ and $C^{18}O$ $J = 2 \rightarrow 1$ emission can only be understood in a model where the UV radiation from the central OB cluster penetrates into a clumpy neutral cloud. Any model which involves a homogeneous distribution of molecular material near the interface can be excluded by the present data. Indeed the arguments given in § III*b* show that the material in the interface has to be clumpy with a surface-to-volume ratio more than an order of magnitude larger than in a homogeneous cloud.

If the individual clumps have high enough column density to completely absorb the UV radiation hitting them, the UV flux originating from the central OB cluster gets blocked by the clump cores and redistributed in angle due to dust scattering. At radius R it is attenuated to the average value

$$F = L/(4\pi R^2) \exp\left[-(\Phi_v/D_c)(R - R_0)\right], \quad (3)$$

where Φ_v and D_c are the volume filling factor and the diameter of the clumps and R_0 is the radius of the H II region. R_0 can be estimated from the measured [C II] distribution to be 1.8 pc. The total luminosity of the exciting star cluster is well known (6×10^6 $L_\odot$), and we take half of its total intensity to contribute to the UV flux. From the fast variation of the CO $J = 2 \rightarrow 1$ and $3 \rightarrow 2$ line profiles (this paper and Rainey *et al.* 1987), the size scale of clumps is ≤ 0.5 pc. The volume filling

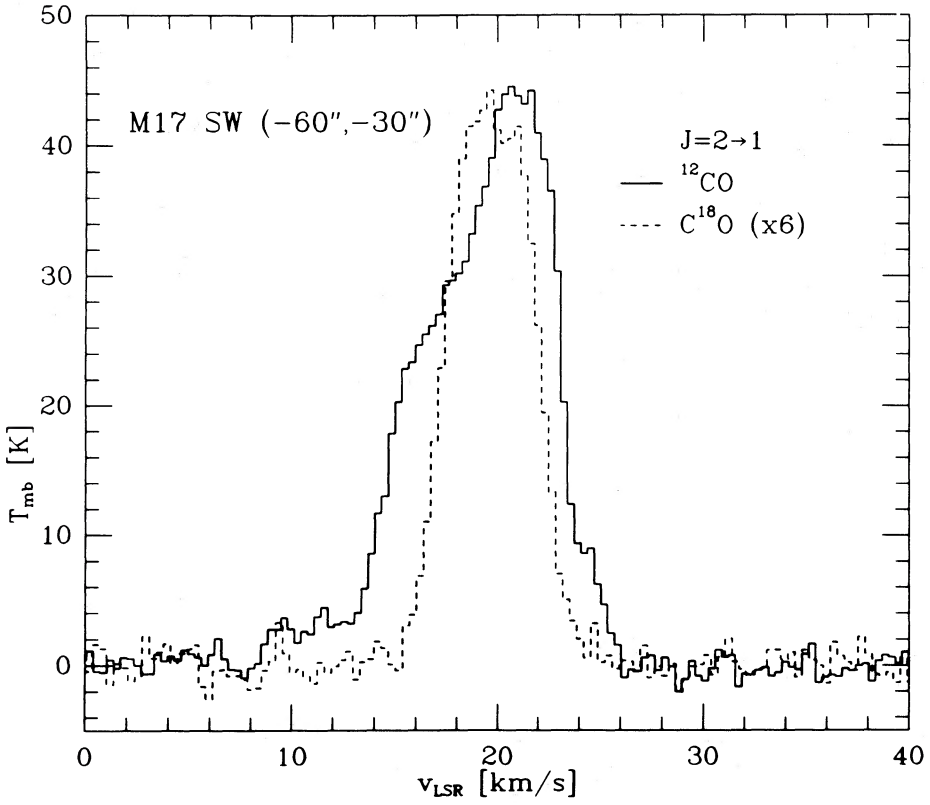

FIG. 10*a*

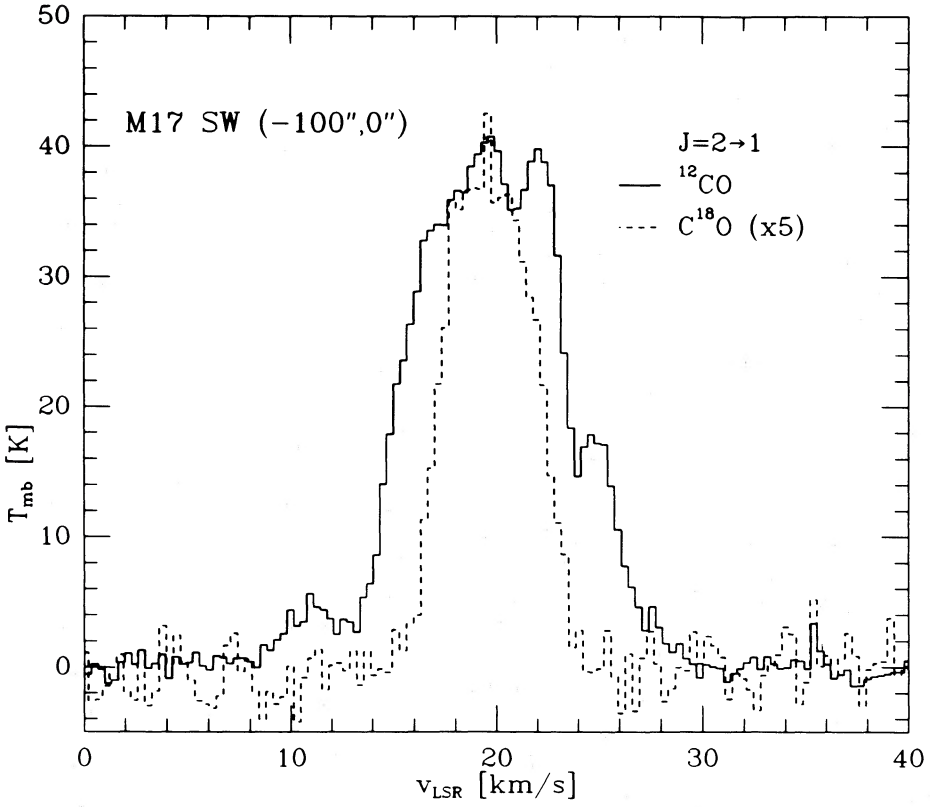

FIG. 10*b*

FIG. 10.—Overlay of ^{12}CO and C^{18}O $J = 2 \rightarrow 1$ spectra toward the positions of peak CO $J = 7 \rightarrow 6$ emission in M17: (*a*) position (60W, 30S), (*b*) position (100W, 0S). The asymmetric and irregular shape of the ^{12}CO profiles indicates that the source has a rather complex internal structure.

factor is between 0.1 and 0.4 from comparison of beam-averaged column densities and source size to the densities required for the excitation of the submillimeter and far-infrared CO lines. The $1/e$ penetration depth of UV radiation in the clumpy cloud model, D_c/Φ_v, is then around 1–2 pc.

[C II] intensity distribution as a function of distance from the central cluster can be computed from equation (3), using the model calculations by Tielens and Hollenbach (1985) and Takahashi, Tielens, and Hollenbach (1987) for conversion of UV energy density to [C II] flux. The number of clumps per beam follows from the assumed volume filling factor and diameter of the clumps, the source distance, and an assumed length along the line of sight of the cloud of 5 pc. As mentioned above, this approach (model I in the following) assumes that the incident UV radiation comes from an extended source or is completely redistributed in angle due to scattering by dust. The opposite extreme case for the attenuation of the UV radiation is based on the assumption that the UV radiation is completely blocked if it hits a clump, but shines straight through otherwise. The dilution of the UV intensity with distance R from the OB cluster then follows $F = L/(4\pi R^2)$, and the fraction of clumps being hit by UV radiation decreases according to the exp $[-\Phi_v/D_c(R - R_0)]$ law (model II in the following).

The resultant [C II] distributions, convolved to the 50″ resolution of the observations, are plotted in Figure 11. Models I and II, describing the extreme cases for the UV flux distribution, bracket the observed [C II] distribution and absolute intensity. A more realistic model will lie in between and therefore fit the observed [C II] distribution even better. Northeast of the H II region, where the [C II] intensity drops off more slowly, a somewhat larger value of $D_c/\Phi_v = 3$ pc provides a reasonable fit to the observed distribution.

The clumpiness of the interface also gives a straightforward explanation for the coexistence of warm CO emission and peak molecular column density (as measured by $C^{18}O$). The warm CO emission arises from the surface of high-density clumps in the interface. Most of the column density is contained in the cooler cores of these clumps. A similar model also applies to the neutral circumnuclear ring in the Galactic center (Genzel *et al.* 1985; Güsten *et al.* 1987).

VI. LOW-LEVEL EXTENDED [C II] EMISSION: CLUMPY STRUCTURE AND ULTRAVIOLET RADIATION THROUGHOUT THE MOLECULAR CLOUD?

The low-level extended [C II] emission is well correlated with the ^{12}CO $1 \rightarrow 0$ emission in the first core of a chain of giant molecular cloud condensations southwest of M17 (Fig. 6; Elmegreen and Lada 1976; Elmegreen, Lada, and Dickinson 1979). The [C II] intensity is about 20 times higher than expected for a single molecular cloud surface illuminated by the average UV field in the solar neighborhood (see the models of Takahashi, Tielens, and Hollenbach 1987). What is the origin of this 15 pc scale [C II] emission?

The M17 H II region illuminating the cloud from the northeast almost certainly cannot explain the intensity level of the extended [C II] emission even if a special geometry is considered. Even the $1/R^2$ dilution of the UV field does not leave enough UV photons at distances greater than 10 pc to account for the observed intensity level. The models discussed above, with a $(1/R^2)$ exp $[-\Phi_v/D_c(R - R_0)]$ dilution, fail to explain

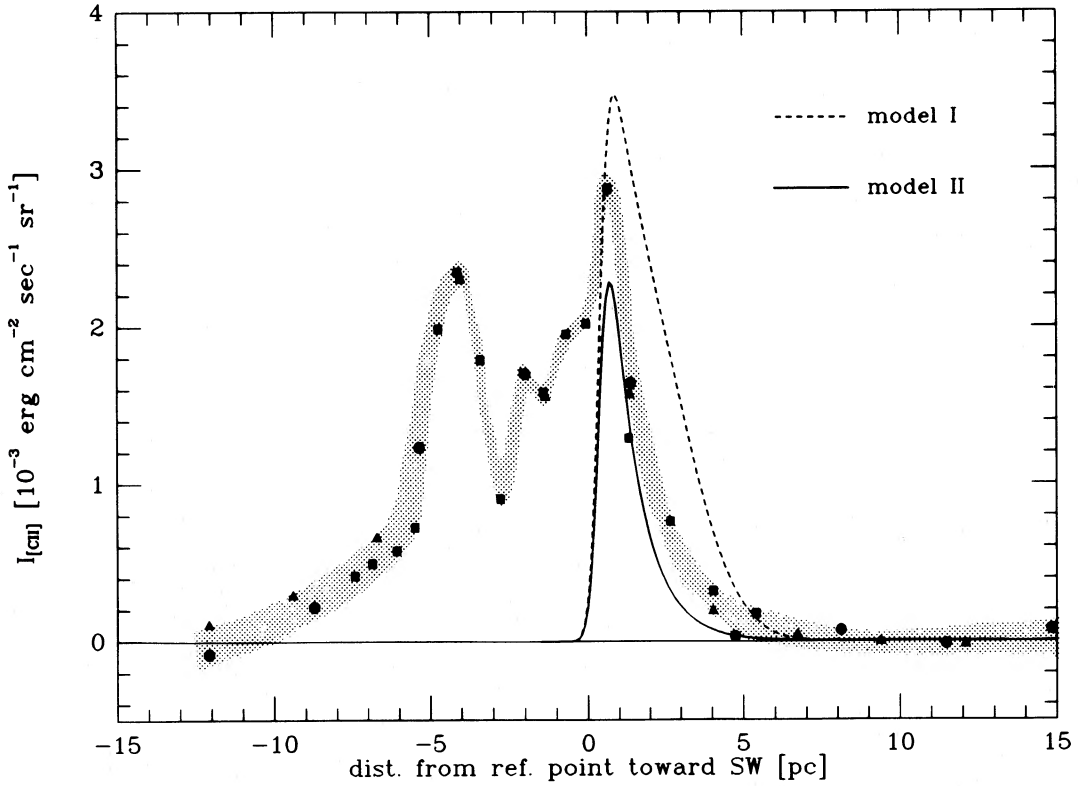

FIG. 11.—Theoretical models (*see text*) for the [C II] intensity distribution for a clumpy molecular cloud penetrated from the side by UV radiation, superposed on the measured [C II] distribution. The extended [C II] emission level of around 5×10^{-4} ergs cm^{-2} s^{-1} sr^{-1} (Fig. 4) has been subtracted.

any measurable [C II] intensity beyond a distance of 5 pc (see Fig. 11). None of the models can explain the flat shape of the extended [C II] emission over the region of 5–15 pc from the M17 SW interface.

As mentioned above, there is also no known mechanism other than photodissociation which can produce the large-scale C^+ region. Excepting the M17 H II region, there are no other strong radio continuum sources in M17 SW which would indicate the presence of ionizing O stars in the molecular cloud (Altenhoff *et al.* 1978). In any case, for UV radiation to penetrate to such large scales, the molecular cloud has to be clumpy throughout. Independent evidence for clumpiness of molecular clouds on large scales comes from the ^{13}CO work by Pérault, Falgarone, and Puget (1985, 1986).

Embedded B type stars are additional sources of 912–1101 Å UV flux, which could be responsible for the enhanced [C II] emission throughout the cloud. Jaffe, Stier, and Fazio (1982) have found several embedded far-infrared/radio continuum sources in the M17 SW molecular cloud complex. They may actually be clusters of B stars (Jaffe *et al.* 1984). The flux detection limits of their balloon-borne far-infrared observations allowed detection of sources with a luminosity equivalent to a zero-age main-sequence B2 star or greater. In their survey there are no sources other than the M17 H II region within 5 pc distance of the extended C II scan. The *IRAS* survey lists nine point sources within the region of the first molecular cloud SW of M17 with a 60 μm–to–25 μm flux ratio greater than 0.4. Their total luminosities of around 500 to 1300 $L_\odot$ are consistent with the exciting objects being embedded B stars. Due to the presence of extended emission in this region, the *IRAS Point Source Catalog* (1985) is severely confusion limited and there may be more embedded B stars present.

Indeed, taking the total mass of the first molecular cloud SW of M17 of 10^5 $M_\odot$ (Elmegreen and Lada 1976), a star formation efficiency of 10%, and a Miller-Scalo initial mass function $\propto M^{-1.35}$ with a low-mass cutoff at 0.2 $M_\odot$, we estimate that ~ 100 B stars should form in the M17 SW cloud. Perhaps half of them may have formed already. Due to the confusion limit in the *IRAS* survey the theoretically estimated number of ~ 50 B stars in the cloud is not in conflict with the observed number. The total luminosity of these stars of $L = 5.6 \times 10^4$ $L_\odot$ (calculated with a mass-luminosity relation $L \propto M^{2.85}$) would create an average energy density $\epsilon = L/(\pi c r^2)$ of ~ 10 times that of the average interstellar radiation field (where $r = 3$ pc is the radius of the whole cloud). Considering that about one-half to one-quarter of the B star luminosity is in the UV range, the estimated number of embedded B stars provide just about enough UV radiation to explain the extended [C II] emission (using the UV flux to [C II] intensity conversion given by Takahashi, Tielens, and Hollenbach 1987). If, in addition, the whole cloud is clumpy or filamentary in structure as suggested by the smoothness of the extended [C II] emission, resulting in 4–6 photodissociation interfaces per beam, less than the theoretically estimated number of embedded B stars and only a factor of 2 more than the ones found in the *IRAS* survey will be enough to explain the extended [C II] emission level. Similarly we predict the presence of extended, low-level [C II] emission in all giant molecular clouds. Finally, the observed large-scale correlation between [C II] and CO $J = 1 \rightarrow 0$ emission may be another consequence of the inferred UV radiation inside molecular clouds.

Alternatively, the UV radiation could be external if the radiation field near M17 is about 4–10 times higher than in the solar neighborhood.

a) Consequence for the Distribution of Neutral Atomic Carbon

The M17 SW cloud appears to be penetrated by UV radiation that ionizes carbon. The same UV radiation will also dissociate CO and sustain a substantial abundance of neutral atomic carbon. The [C I] fine-structure line intensity predicted by photodissociation models (Tielens and Hollenbach 1985; Takahashi, and Hollenbach 1987) is relatively insensitive to UV energy density. In a clumpy medium the [C I] emission should therefore count the number of interfaces per beam. Optically thin, isotopic CO lines trace column density, and hence, with a typical average column density per clump, essentially count the number of clumps per beam in a clumpy cloud. Hence, there should be a correlation between the spatial distributions of [C I] and isotopic CO lines.

Keene *et al.* (1985) find a good spatial correlation between ^{13}CO $1 \rightarrow 0$ and [C I] $^3P_1 \rightarrow {}^3P_0$ emission on a scale size of 3′ (~ 2 pc), consistent with that prediction. However, it is not clear how much of the observed [C I] emission originates in an enhanced emission region near the interface and how much of the emission comes from extended emission throughout the cloud. Both higher spatial resolution and more extended [C I] observations are desirable in order to settle the question of [C I] abundance and distribution in M17.

VII. A PHYSICAL MODEL FOR THE MOLECULAR GAS IN M17 SW

The warm molecular material traced in the CO submillimeter and far-infrared transitions (temperature a few 10^2 K) and the lower J ^{12}CO lines, having brightness temperatures around 35–55 K, cannot originate in the same gas component. In order to understand the structure of the molecular gas in the interface we will present in the following a comparison of the profiles of different CO and other molecular lines at the CO $J = 7 \rightarrow 6$ peak position (60W, 30S).

At this position comparison spectra are available in the transitions of ^{13}CO $J = 1 \rightarrow 0$ and $J = 2 \rightarrow 1$ (Plambeck, private communication), ^{12}CO and $C^{18}O$ $J = 2 \rightarrow 1$ (this paper), ^{12}CO $J = 3 \rightarrow 2$ (Rainey *et al.* 1987), ^{12}CO $J = 4 \rightarrow 3$ (Schulz and Krügel 1987), and ^{12}CO $J = 7 \rightarrow 6$ lines (this paper). In addition, there are spectra of the NH_3 $(J, K) = (1, 1)$ and (2, 2) inversion lines (Güsten, private communication). The spectra are overlaid in Figures 12 and 13.

a) Observational Facts

Any quantitative model of the molecular cloud/H II region interface in M17 SW has to account for the following observational facts:

1. *There is a significant amount of warm* CO *gas in the interface.* The main-beam brightness temperature of the CO $7 \rightarrow 6$ line of 85 K implies a kinetic temperature of the warm and dense gas of at least 100 K. The CO $14 \rightarrow 13$ intensity at a level only slightly weaker than the CO $7 \rightarrow 6$ line implies the presence of even warmer gas (T around 200–400 K). The density required to excite the high J CO lines is around several 10^4 cm^{-3}. The CO column densiity in this warm material is around a few 10^{18} cm^{-2}.

2. *There are remarkable variations in line profile and strength with J for the* ^{12}CO *transitions.* The $J = 1 \rightarrow 0$, $2 \rightarrow 1$, $3 \rightarrow 2$, and $4 \rightarrow 3$ lines have peak main-beam brightness temperatures of 55, 45, 25, and 35 K, respectively. The line profiles are asym-

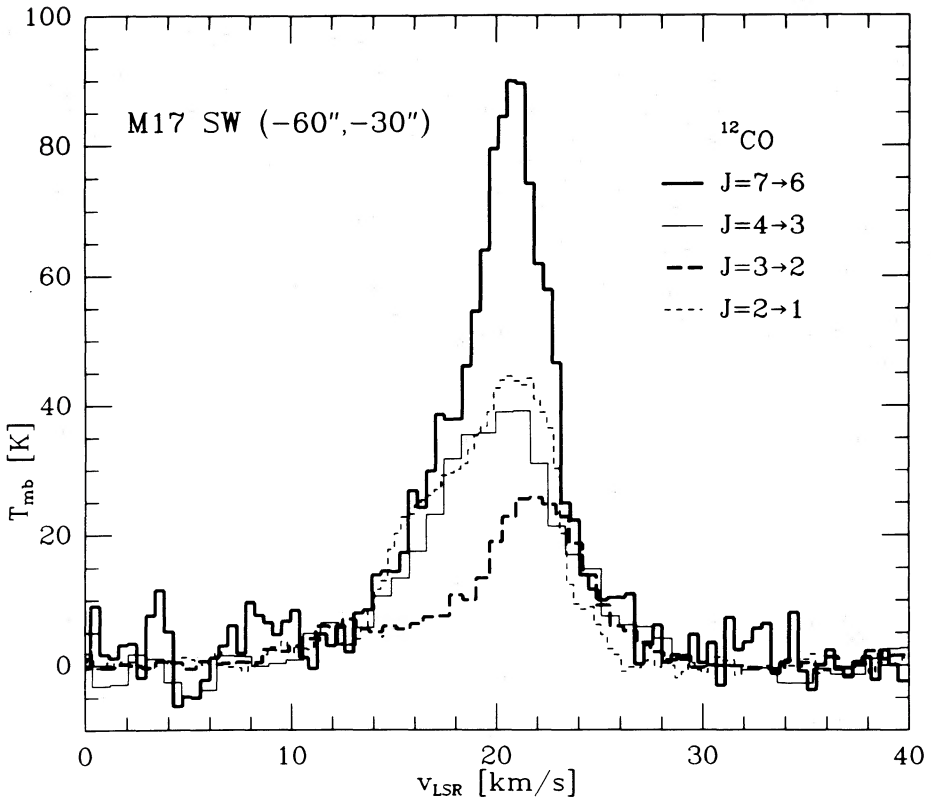

FIG. 12*a*

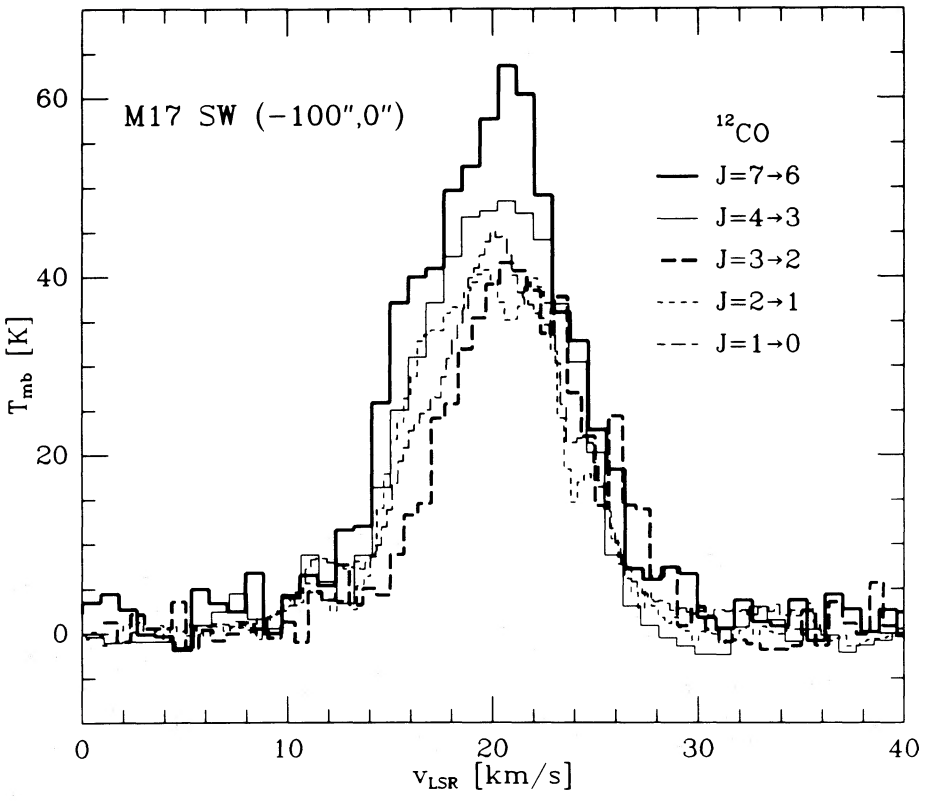

FIG. 12*b*

FIG. 12.—^{12}CO millimeter and submillimeter spectra at the two peak positions of CO $J = 7 \rightarrow 6$ emission: (*a*) position (60W, 30S), (*b*) position (100W, 0S). The $J = 1 \rightarrow 0$ spectrum is from Plambeck (private communication), the $J = 3 \rightarrow 2$ spectra are from Rainey *et al.* (1987), the $J = 4 \rightarrow 3$ spectra are from Schulz and Krügel (1987), the $J = 2 \rightarrow 1$ and $7 \rightarrow 6$ spectra are from this paper.

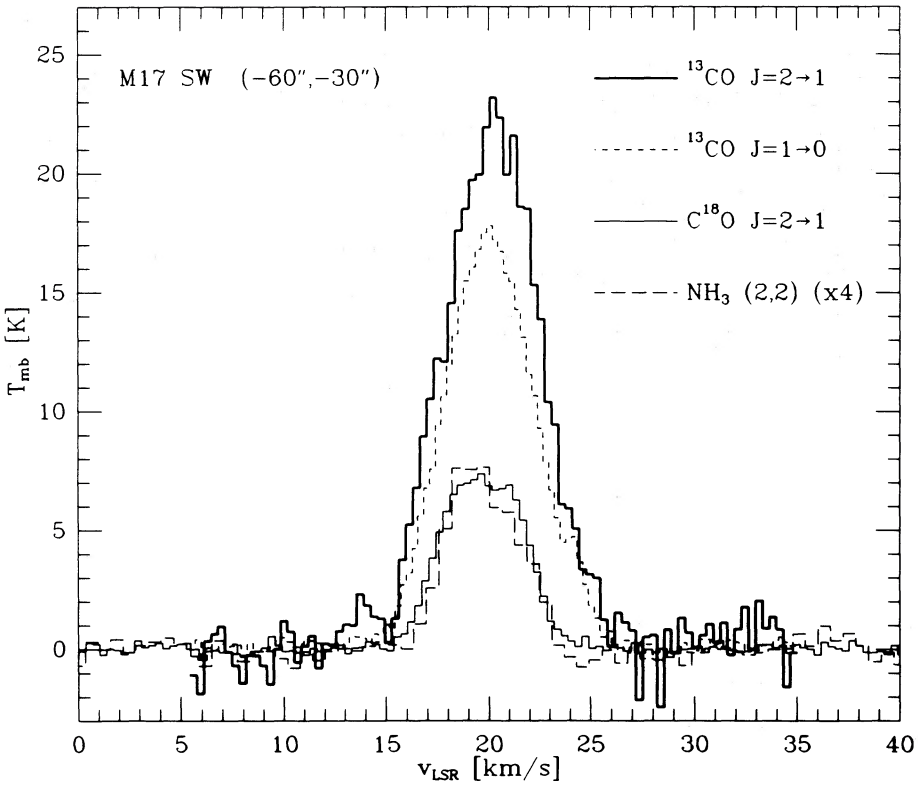

FIG. 13*a*

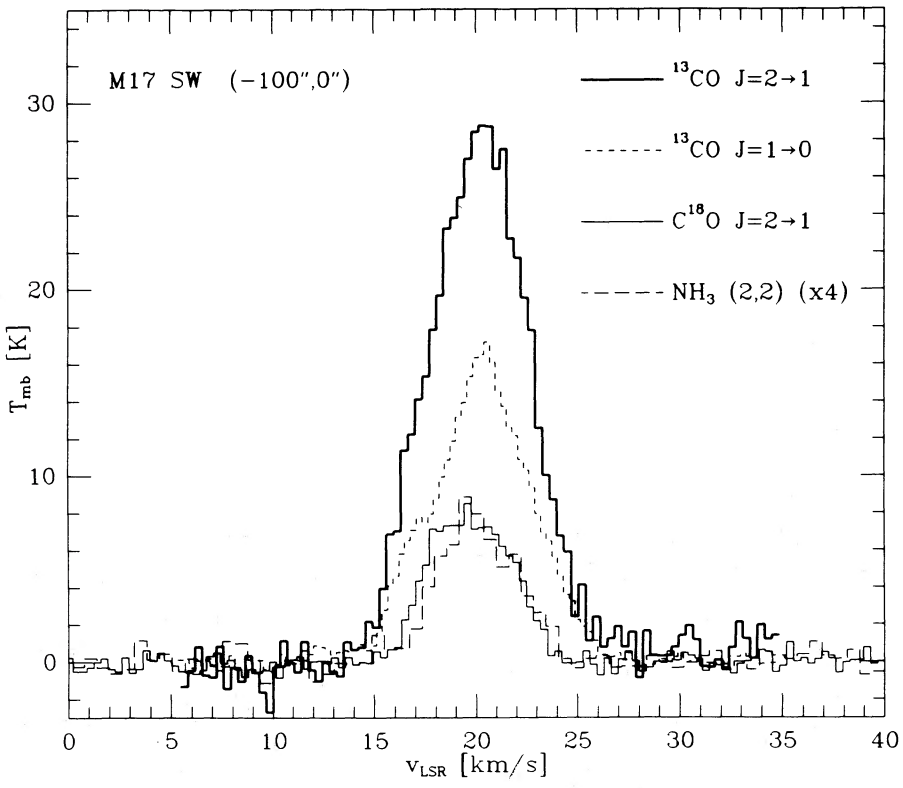

FIG. 13*b*

FIG. 13.—Comparison of isotopic CO (C^{18} $J = 2 \rightarrow 1$, this work; ^{13}CO, Plambeck, private communication) and NH_3 $(J, K) = (2, 2)$ spectra (Güsten, private communication) at the two peak positions of CO $J = 7 \rightarrow 6$ emission: (*a*) position (60W, 30S), (*b*) position (100W, 0S).

metric with the low-velocity shoulder being weaker than the high-velocity shoulder. This effect is strongest in the $J = 3 \rightarrow 2$ line, where the peak is effectively shifted to a velocity of 23 km s^{-1}. The profiles in the line wings are (except for the heavily affected $3 \rightarrow 2$ line) very similar to the $J = 7 \rightarrow 6$ line. The very bright and narrow line center of the $7 \rightarrow 6$ line, however, seems to be missing in the lower J lines. In contrast, the lower J isotopic CO line profiles are simple symmetric, almost Gaussian, profiles centered at $v_{LSR} = 20$ km s^{-1} (Fig. 13).

3. *Most of the column desnsity is in gas of temperature* ~ 50 K. The ammonia $(J, K) = (1, 1)$ and $(2, 2)$ lines (Güsten, private communication) are optically thin at the interface, as determined from the hyperfine satellite intensity in the (1, 1) line. Their profiles are very similar to the optically thin isotopic CO lines (Fig. 13). This is to be expected as both trace the material with the highest overall column density. The NH_3 rotational temperature T_R in the optically thin limit is

$$T_R = -42/\ln [0.283 T_B(2, 2)/T_B(1, 1)] = 35 \text{ K}, \quad (4)$$

corresponding to a kinetic temperature of 50 K (Walmsley and Ungerechts 1983; Stutzki and Winnewisser 1985). The total ammonia column density is 3×10^{14} cm^{-2}. Comparison with the column density derived from the optically thin isotopic CO lines (see § IV*b*) gives an $[NH_3]/[CO]$ abundance of 4×10^{-5}, a value which is on the low side of the range typically observed, but which agrees reasonably well with chemical model predictions (Graedel, Langer, and Frerking 1982). The ammonia lines thus indicate that the material traced by the isotopic CO lines has a kinetic temperature of around 50 K.

The situation is similar at position (100W, 0S), close to the far-infrared 100 μm peak (Figs. 12*b* and 13*b*). The ^{12}CO lines, including CO $7 \rightarrow 6$, are wider than the isotopic CO lines and the NH_3 profiles. The brightness temperatures of the $J = 1 \rightarrow 0$, $2 \rightarrow 1$, and $3 \rightarrow 2$ ^{12}CO lines are about the same. The $J = 4 \rightarrow 3$ line is already slightly brighter, and the $J = 7 \rightarrow 6$ peak brightness temperature of 65 K is around 30% higher than that of the lower J lines.

To fit all these observational data in a consistent model of the molecular material in the H II region/molecular cloud interface requires several gas components with a range of temperature, density, and column density. In the following we present an outline of a possible solution.

b) A Two-Component Model as a First Approach: Ultraviolet-heated Warm Gas at the Surface of Denser and Cooler Clumps

There must be at least two gas components present in the molecular cloud/H II region interface. A warm ($T \approx$ several 100 K), dense component is traced by the CO $7 \rightarrow 6$ and $14 \rightarrow 13$ lines and contributes 5%–20% of the total CO column density. A cool ($T \approx 50$ K), dense component of large column density is traced by the isotopic CO lines and NH_3 (1, 1) and (2, 2). The optical depth of the warm, dense component in the lower J isotopic lines ($\tau[\text{warm}] \leq 10^{-1}$) is much too low to account for the observed brightness of the isotopic CO lines.

Both components are optically thick in the $3 \leq J \leq 7$ ^{12}CO lines. Since the warm, dense gas appears to dominate the emission of the ^{12}CO $J = 7 \rightarrow 6$ line in spite of the high optical depth of the cool gas in this transition ($\tau_{7 \rightarrow 6}[\text{cool}] \approx 100$), the warm material has to be in front of, or around, the cool material. The excitation of this material is most reasonably explained by UV heating through photoelectrons off dust grains (Harris *et al.* 1987*b*). A likely physical model is thus UV-heated warm gas at the surfaces of dense clumps or filaments. This picture is supported by the interpretation of the [C II] emission distribution as originating in a clumpy interface. Because of its relatively low column density, the warm and dense component contributes little to optically thin transitions ($C^{18}O$, NH_3, or CS). This is consistent with the observations (Güsten, private communication; Snell *et al.* 1984; Snell *et al.* 1986).

c) Evidence for a Third Component of Molecular Gas

It is not possible to fully explain the intensities and line profiles of the low-J ^{12}CO lines in the two-component model described above. Any gas component with the temperature and density required to explain the observed CO $7 \rightarrow 6$ and $14 \rightarrow 13$ intensities has a CO $4 \rightarrow 3$ intensity higher than that observed by a least 50%. In addition, a two-component model cannot explain the intensity variation with J in the lower J lines, especially the low peak brightness temperature of 25 K in the $J = 3 \rightarrow 2$ line at position (60W, 30S) and the different shapes of the line profiles, again especially prominent in the $J = 3 \rightarrow 2$ line.

Large systematic uncertainties in the calibration of the different ^{12}CO millimeter and submillimeter lines could perhaps explain the inconsistencies in the integrated intensities. They cannot, however, explain the variation in line profile. If the uncertainties in intensity calibration are as quoted by the different observers, the only way to understand the intensity distribution with J and the variation of the line profiles is that the emission from warm gas is partially absorbed in much cooler ($T \approx 30$ K) foreground gas. In the low-J lines, optical depth increases proportionally to J^2 up to a maximum J beyond which the opacity decreases at least exponentially (in the thermalized case) or faster (in the case of subthermal population) due to insufficient population in the high-J states ($J > 4$) so that more and more emission from the brighter background shines through. A quantitative model has to also take into account the optical pumping of the CO transitions in the cooler gas by the strong emission of the warm gas. Collisions in the foreground gas component then cool the gas against the line heating from the warm background. Depending on clumpiness and other geometrical effects this radiative coupling can be more or less important.

The cool, absorbing foreground component must have a velocity dispersion comparable to the warm gas, i.e., 5–10 km s^{-1}. Otherwise there should be narrow self-absorption dips in the profiles. The asymmetry in the most heavily affected ^{12}CO $J = 3 \rightarrow 2$ profile indicates that the center velocity of the absorbing material is slightly lower than that of the bulk of the cloud. Its column density must be rather low in order to have its optical depth changing rapidly with J. Too large a column density will result in all lines being optically thick, so that the observed Planck brightness temperature would be constant and equal to the low kinetic temperature of the absorbing component. Assuming that the foreground component is almost optically thick in the ^{12}CO $J = 3 \rightarrow 2$ line, its kinetic temperature has to be about 30 K, that is, equal to the peak brightness temperature of the $3 \rightarrow 2$ line.

d) A Possible Three-Component Model

The following physical model for the H II region/molecular cloud interface may be considered as a first approach to com-

bining all data available from different molecular species and transitions.

The molecular cloud consists of a large number of ~0.3–0.6 pc diameter clumps, sheets, or filaments. The clumps have internal temperatures near 50 K and are heated by collisions with embedded warm dust. The clump density is several 10^4 cm^{-3} or greater. The highest density cores ($>10^5$ cm^{-3}) of the clumps represent the material traced in CS (Snell *et al.* 1984; Snell *et al.* 1986). These clumps also produce the observed NH_3 emission and the optically thin isotopic CO lines. The 50 K clump material accounts for a few times 10^{23} cm^{-2} H_2 column density.

UV radiation from the M17 OB cluster penetrates the clumpy molecular material and creates photodissociation regions on the clump surfaces. CO gas at the surfaces is heated to a temperature of several hundred degrees via the photoelectric effect. This component is the warm, dense gas traced by the CO $J = 7 \rightarrow 6$ and $14 \rightarrow 13$ lines. The warm, dense gas accounts for a beam-averaged H_2 column density of a few times 10^{22} cm^{-2}, or 5%–20% of the material in the clump cores. Due to its high temperature, the optical depth of the low-J isotopic CO lines in this component is rather low, and it does not contribute to the emission in the low-J isotopic lines. Similarly, the optical depth of the NH_3 lines from this component is too low to contribute substantially to the observed emission.

The third component necessary to explain the observations is a cool component that partially absorbs the emission from the two other components, the clump cores and photodissociation surfaces of the clumps, in the ^{12}CO low-J lines. In order to produce the rapid variation of the absorption with J, peaking at $J = 3 \rightarrow 2$, this component has to have a rather low temperature of around 30 K and a very low CO column density of around 2×10^{17} cm^{-2}, only a few percent of the total material. The line width has to be comparable to the line width in the clumps and clump surfaces in order to avoid self-absorption dips. It is thus likely that the material is physically related to the clumpy medium. The third component may be cool material from the envelopes of other clumps along the line of sight which avoid photoheating due to the shadowing of UV radiation.

e) *A Simple Radiative Transfer Model*

In order to quantify this model we calculated escape probability radiative transfer models that take into account the radiative interaction between the different components by treating the line emission of the other components as background radiation for the component presently being calculated. After several interactions between the different components the populations converge to a solution for the three radiatively coupled layers.

We discuss in detail the results for position (60W, 30S). The results for position (100W, 0S) are qualitatively similar, although due to the weaker variation of ^{12}CO line brightness with J at this position a slightly warmer ($T \approx 40$ K) foreground component with somewhat higher column density can explain the observations. We get a fit to all observed CO lines within 25%. Figure 14 displays the results for position (60W, 30S). Table 1 summarizes the parameters. This model has the clump cores surrounded by the photodissociation "envelopes," that radiate back into the cores with a solid angle of 4π or a coupling factor of 1. The clump cores couple back into the envelopes with a coupling factor of 0.5, and the combined emission of the clump core and envelope couple to the foreground cloud with a solid angle coupling factor of 0.3. The absorbing foreground layer (component 3) is assumed to fill the beam, the clump cores and envelopes are assumed to have a beam filling factor $\eta_f = 70\%$. The observed intensity is then η_f times the intensity of component 1 and 2 seen through component 3, plus $(1 - \eta_f)$ times the emission of component 3 alone. The parameters of both cloud cores and envelopes are very well constrained by the CO $7 \rightarrow 6$-to-$14 \rightarrow 13$ intensity ratio and the isotopic low-J CO emission as discussed above. The parameters for the foreground absorbing layer are fixed by the variation of line brightness temperature with J in the lower J ^{12}CO lines.

f) *Consequences of the Modeling Result*

The radiative coupling is most important for the diffuse foreground cloud, where the bright CO lines from the clump envelopes pump the population to temperatures substantially higher than the kinetic temperature. A density of close to 10^4 cm^{-3} is required to collisionally cool the gas against this radiative pumping. Alternatively, the absorbing material has to be far enough away from the clumps, so that radiative coupling is less important. It is then, however, difficult to understand the similar line widths in all three components. The low column density is necessary to obtain the strong variation of absorption with J. In the model presented, $\tau(^{12}CO)$ in the absorbing layer varies from 0.6 to 1.8 between $J = 1 \rightarrow 0$ and $J = 3 \rightarrow 2$. The low kinetic temperature of the absorbing layer is necessary to keep the absorption down in the CO $7 \rightarrow 6$ line, which has already an optical depth of 0.4 in the specific model presented here.

The model thus shows that the three components of gas quoted above can account for the observed CO intensities, whereas the two-component model cannot. Clearly, the actual situation will be much more complex. For one, the definition of three distinct temperature and density regions is somewhat arbitrary: in reality there must be a distribution over temperatures and densities in the range covered by those three components. As the ^{12}CO lines have very high opacity, any small amount of additional material has an important effect on the observed emission.

Second, no attempt has been made to explain the line profile and its variation between the different isotopic lines. The

TABLE 1

RADIATIVE TRANSFER MODEL RESULTS FOR CO

Physical Parameter	Component 1 (Clump Cores)	Component 2 (Clump Envelopes)	Component 3 (Absorbing Layer)
T_{kin} (K)	50	200	25
n_{H_2} (cm^{-3})	5×10^4	3×10^4	3×10^4
$N_{CO}/\Delta v$ (cm^{-2} [10 km s^{-1}]$^{-1}$)	5×10^{19}	6×10^{18}	2×10^{17}

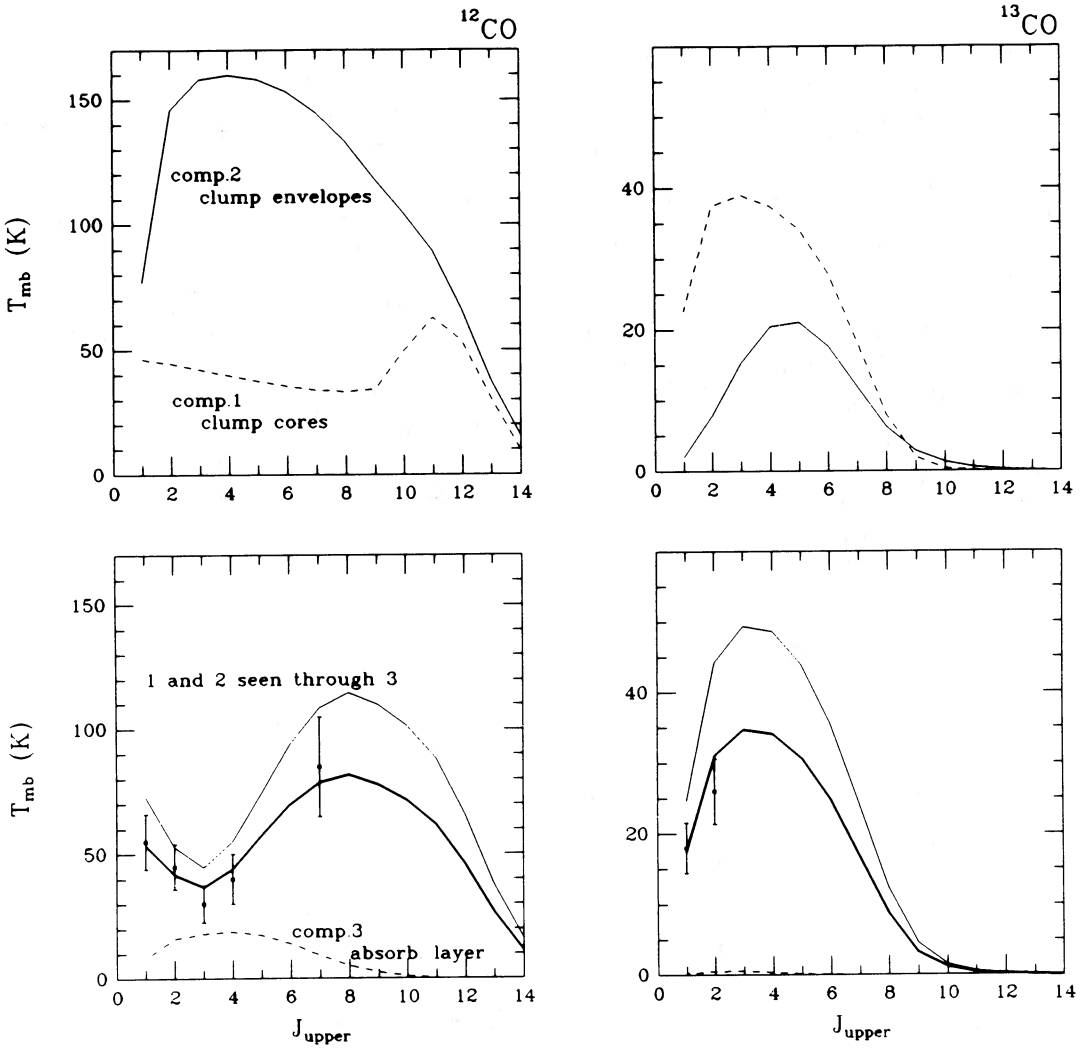

FIG. 14.—Results of three-component radiative transfer modeling (*see text*) of the millimeter and submillimeter CO emission at position (60W, 30S). The left side shows ^{12}CO, the right ^{13}CO. The top shows the intrinsic brightness temperature distribution of transition $J \rightarrow J - 1$ vs. J for components 1 and 2, the cool clump cores (*solid line*) and warm clump envelopes (*dashed line*), respectively. For ^{12}CO the warm, dense gas in the envelopes dominates the emission, for ^{13}CO the clump cores dominate due to their larger column dennsity. Note the radiative heating of the core component by line radiation from the envelopes for $J \geq 9$, where the collisions are too slow to cool the gas against the line heating. The bottom graph shows the intrinsic emission from the foreground absorbing layer (component 3, *dashed line*) and the total brightness temperature distribution of components 1 and 2 seen through this layer (*thin solid line*). A good fit to the observed points for both ^{12}CO is obtained with the assumption that the clump cores and envelopes fill 70% of the beam area, whereas the foreground layer is extended (*heavy solid lines*).

profile contains important information on the structure of the molecular material in the interface, especially with regard to clumpiness. Martin, Sanders, and Hills (1984) give a detailed discussion of the effect of radiative transport in a macroturbulent clumpy medium on the line profiles. A more realistic description of the molecular emission in the M17 H II region molecular cloud interface will have to take these effects into account.

The multicomponent modeling indicates how sensitive the medium-J ^{12}CO lines are to radiative transport and self-absorption by relatively small amounts of gas. Further submillimeter observations of isotopic CO lines will also have to be interpreted with great care. Due to its much higher column density the cool gas in the clump cores can easily dominate the emission in the submillimeter isotopic CO lines. The model discussed here for M17 (50W, 30S), for example, predicts a brightness temperature of 25 K in the ^{13}CO $J = 6 \rightarrow 5$ line (Fig. 14), about a third of the ^{12}CO $6 \rightarrow 5$ peak brightness temperature. Of its intensity, however, 65% comes from the cool 50 K cloud cores, and only 35% originates in the warm dense gas that dominates the ^{12}CO $J = 7 \rightarrow 6$ emission.

VIII. SUMMARY

The large-scale spatial distribution of the [C II] emission around M17 SW shows that the UV radiation from the H II region penetrates into the neutral molecular material to a much larger depth than is consistent with a uniform distribution of matter. The molecular cloud has to have a clumpy or filamentary structure resulting in a UV attenuation length of around 2 pc in the dense cloud core to the southwest of the M17 H II region. Strong [C II] emission originates in photodissociation surfaces on molecular clumps and partly in high-density atomic condensations associated with the ionization front. The observed [C II] intensity at the H II region/molecular cloud interface is consistent with the known total luminosity of the exciting group of OB stars and the photo-

dissociation models of Tielens and Hollenbach (1985) and Takahashi, Tielens, and Hollenbach (1987).

The UV radiation from the M17 OB cluster affects the molecular cloud to a depth of around 5 pc. In addition, there is evidence for a constant, low level of [C II] emission throughout the first molecular cloud SW of M17. The presence of this extended [C II] emission requires a clumpy structure of, and an enhanced average UV field throughout, the cloud. The UV intensity necessary to explain the extended [C II] emission level can be created by about 20–50 B stars. This number of embedded B stars is also expected to be present in the cloud according to standard values for star formation efficiency and initial mass function. As a consequence of the penetration of the whole cloud by UV radiation, we predict a low level of neutral carbon fine-structure emission throughout the cloud core. In addition, we expect a peak of [C I] emission from the clumpy interface region. The [C I] data presently available (Keene *et al.* 1985) are probably consistent with this scenario.

The new far-infrared and submillimeter data show the presence of dense, very warm (densities several 10^4 cm^{-3}, temperatures several hundred degrees) atomic and molecular gas in the interface between H II region and the cooler molecular cloud. The warm molecular component may be heated by photoelectrons off dust grains. A comparison of the available data in different molecular lines confirms the picture of a clumpy interface region and suggests the presence of several gas components with temperatures ranging from several ten to several hundred degrees and a comparable velocity dispersion of ≥ 5 km s^{-1} throughout this temperature range.

We thank the staff of the Kuiper Airborne Observatory for their enthusiastic support. We are grateful to C. H. Townes for valuable discussion and help with the airborne observations, to E. E. Becklin for support and assistance with the observations made with the University of Hawaii 88 inch telescope, to John Howe for help with the Kitt Peak observations, to R. Güsten and R. Plambeck for giving us access to data prior to publication, and to J. Wouterloot for help with the *IRAS* data base. This research was in part supported by NASA grant NAG 2-208 and by the Presidential Young Investigator's Award to R. Genzel (NSF grant AST83-51381 and a grant from Rockwell International).

REFERENCES

Altenhoff, W. J., Downes, D., Pauls, T., and Schraml, J. 1978, *Astr. Ap. Suppl.*, **35**, 23.
Beetz, M., Elsässer, H., Poulaka, C., Weinberger, R. 1976, *Astr. Ap.*, **50**, 41.
Chini, R., Elsässer, H., and Neckel, Th. 1980, *Astr. Ap.*, **91**, 186.
Clavel, J., Viala, Y. P., and Bel, N. 1978, *Astr. Ap.*, **65**, 435.
Crampton, D., Georgelin, Y. M., and Georgelin, Y. P. 1978, *Astr. Ap.*, **66**, 1.
Crawford, M. K., Genzel, R., Townes, C. H., and Watson, D. M. 1985, *Ap. J.*, **291**, 755.
Crawford, M. K., Lugten, J. B., Fittelson, W., and Genzel, R. 1986, *Ap. J. (Letters)*, **303**, L57.
de Jong, T., Dalgarno, A., and Boland, W. 1980, *Astr. Ap.*, **91**, 68.
Elliot, K. H., and Meaburn, J. 1975, *Ap. Space Sci.*, **35**, 81.
Elmegreen, B. G., and Lada, C. J. 1976, *A.J.*, **81**, 1089.
Elmegreen, B. G., Lada, C. J., and Dickinson, D. F. 1979, *Ap. J.*, **230**, 415.
Evans, N. J., Mundy, L. G., Davis, J. H., and VandenBout, P. 1987, *Ap. J.*, **312**, 344.
Felli, M., Churchwell, E., and Massi, M. 1984, *Astr. Ap.*, **136**, 53.
Gatley, I. R., Becklin, E. E., Sellgren, K., and Werner, M. W. 1979, *Ap. J.*, **233**, 575.
Gatley, I. R., and Kaifu, N. 1987, in *IAU Symposium 120, Astrochemistry*, ed. M. S. Vardya and S. P. Tarafdar (Dordrecht: Reidel), p. 153.
Genzel, R., Watson, D. M., Crawford, M. K., and Townes, C. H. 1985, *Ap. J.*, **297**, 766.
Graedel, T. E., Langer, W. D., and Frerking, M. A. 1982, *Ap. J. (Suppl.)*, **48**, 321.
Gull, S. F. K., and Daniell, G. J. 1978, *Nature*, **272**, 686.
Güsten, R., Genzel, R., Wright, M. C. M., Jaffe, D. T., Stutzki, J., and Harris, A. I. 1987, *Ap. J.*, **318**, 124.
Harper, D. A., Low, F. J., Rieke, G. H., and Thronson, H. A. 1976, *Ap. J.*, **205**, 136.
Harris, A. I., Jaffe, D. T., Silber, M., and Genzel, R. 1985, *Ap. J. (Letters)*, **294**, L93.
Harris, A. I. 1987, MPE Preprint No. 88.
Harris, A. I., Jaffe, D. T., Stutzki, J., and Genzel, R. 1987*a*, *Internat. J. Infrared Millimeter Waves*, Vol. **8**, No. 8, p. 857.
Harris, A. I., Stutzki, J., Genzel, R., Lugten, J. B., Stacey, G. J., and Jaffe, D. T. 1987*b*, *Ap. J.*, in press.
Hill, J. K., and Hollenbach, D. J. 1978, *Ap. J.*, **225**, 390.
Hollenbach, D. J., and McKee, C. F. 1979, *Ap. J. (Suppl.)*, **41**, 555.
Icke, V., Gatley, I. R., and Israel, F. 1980, *Ap. J.*, **236**, 808.
IRAS Point Source Catalog. 1985, Joint *IRAS* Science Working Group (Washington: GPO).
Jaffe, D. T., Güsten, R., and Downes, D. 1981, *Ap. J.*, **250**, 621.
Jaffe, D. T., Harris, A. I., and Genzel, R. 1987, *Ap. J.*, **316**, 231.
Jaffe, D. T., Hildebrand, R. H., Keene, J., Harper, D. A., Loewenstein, R. F., and Moran, J. M. 1984, *Ap. J.*, **281**, 255.
Jaffe, D. T., Stier, M. T., and Fazio, G. G. 1982, *Ap. J.*, **252**, 601.
Jaffe, D. T., *et al.* 1987, in preparation.
Keene, J., Blake, G. A., Phillips, T. G., Huggins, P. J., and Beichman, C. A. 1985, *Ap. J.*, **299**, 967.
Kleinmann, D. E., and Wright, E. L. 1973, *Ap. J. (Letters)*, **185**, L131.
Kurutz, N., Smyers, S., Russell, R. W., Harwit, M., and Melnick, G. 1983, *Ap. J.*, **264**, 538.
Kutner, M. L., and Ulich, B. L. 1981, *Ap. J.*, **250**, 341.
Lada, C. J., Dickinson, D. F., Gottlieb, C. A., and Wright, E. L. 1976, *Ap. J.*, **207**, 113.
Langer, W. 1976, *Ap. J.*, **206**, 699.
Lugten, J. B. 1987, Ph.D. thesis, University of California, Berkeley.
Lugten, J. B., Stacey, G. J., Morris, A. I., Genzel, R., and Townes, C. H. 1986*a*, in *AIP Conf. Proc. 155, The Galactic Center* (New York: ATP), p. 118.
———. 1986*b*, *Ap. J.*, **306**, 691.
Martin, H. M., Sanders, D. B., and Hills, R. E. 1984, *M.N.R.A.S.*, **208**, 35.
Mundy, L. G. 1984, Ph.D. thesis, University of Texas at Austin.
Mundy, L. G., Evans, N. J., Snell, R. L., and Goldsmith, P. F. 1987, *Ap. J.*, **318**, 392.
Mundy, L. G., Snell, R. L., Evans, N. J., Goldsmith, P. F., and Bally, J. 1986, *Ap. J.*, **306**, 670.
Pérault, M., Falgarone, E., and Puget, J. L. 1985, *Astr. Ap.*, **152**, 371.
———. 1986, *Astr. Ap.*, **157**, 139.
Prasad, S. S., and Tarafdar, S. P. 1983, *Ap. J.*, **267**, 603.
Rainey, R., White, G. J., Gatley, I., Hayashi, S. S., Kaifu, N., Griffin, M. J., Monteiro, T. S., Crowin, N. J., and Sciveti, A. 1987, *Astr. Ap.*, **171**, 252.
Russell, R. W., Melnick, G., Gull, G. E., and Harwit, M. 1980, *Ap. J. (Letters)*, **240**, L99.
Russell, R. W., Melnick, G., Smyers, S. D., Kurutz, N. T., Gosnell, T. R., Harwit, M., and Werner, M. W. 1981, *Ap. J. (Letters)*, **250**, L35.
Sanders, D. B., Clemens, D. P., Scoville, N. Z., Solomon, P. M. 1983, *Ap. J.*, **60**, 1.
Schraml, J., and Mezger, P. G. 1969, *Ap. J.*, **156**, 269.
Schulz, A., and Krügel, E. 1987, *Astr. Ap.*, **171**, 297.
Snell, R. L., Mundy, L. G., Goldsmith, P. F., Evans, N. J., and Erickson, N. R. 1984, *Ap. J.*, **274**, 625.
Snell, R. L., Goldsmith, P. F., Ulich, B. L., Lada, C. J., Martin, R., and Schulz, A. 1986, *Ap. J.*, **304**, 780.
Stacey, G. J. 1985, Ph.D. thesis, Cornell University.
Stacey, G. J., Lugten, J. B., and Genzel, R. 1987, in preparation.
Stacey, G. J., Smyers, S. D., Kurtz, N. T., and Harwit, M. 1983*a*, *Ap. J. (Letters)*, **265**, L7.
———. 1983*b*, *Ap. J. (Letters)*, **268**, L99.
Stacey, G. J., Viscuso, P. J., Fuller, C. E., and Kurtz, N. T. 1985, *Ap. J.*, **289**, 803.
Stutzki, J., and Winnewisser, I. 1985, *Astr. Ap.*, **148**, 254.
Takahashi, T., Tielens, A. G. G., and Hollenbach, D. 1987, preprint.

Thronson, H. A., and Lada, C. J. 1983, *Ap. J.*, **269**, 175.
Tielens, A. G. G., and Hollenbach, D. 1985, *Ap. J.*, **291**, 722.
Walmsley, C. M., and Ungerechts, H. 1983, *Astr. Ap.*, **122**, 164.
Watson, D. M. 1984, in *Galactic and Extragalactic Infrared Spectroscopy*, ed. Kessler and Phillips (Dordrecht: Reidel), p. 195.
Watson, D. M., Storey, J. W. V., Townes, C. H., and Haller, E. E. 1981, *Ap. J.*, **250**, 605.
Wilson, T. L., Fazio, G. G., Jaffe, D. T., Kleinmann, D. E., Wright, E. L., and Low, F. J. 1979, *Astr. Ap.*, **76**, 86.

R. GENZEL, A. I. HARRIS, and J. STUTZKI: Max-Planck-Institut für Physik und Astrophysik, Institut für Extraterrestrische Physik, D-8046 Garching bei München, Federal Republic of Germany

D. T. JAFFE: Department of Astronomy, University of Texas, Austin, TX 78712

J. B. LUGTEN: Institute for Astronomy, University of Hawaii, 2680 Woodlawn Drive, Honolulu, HI 96822

G. J. STACEY: Department of Physics, University of California, Berkeley, CA 94720